공학박사 학위논문

A STUDY OF SURFACE POLISHING EFFECTS ON ELECTROWETTING DEVICES

일렉트로웨팅 장치의 표면 평탄화 효과에 관한 연구

2013 년 8 월

서울대학교 대학원

협동과정 바이오엔지니어링 전공

이 충 희

A STUDY OF SURFACE POLISHING EFFECTS ON ELECTROWETTING DEVICES

일렉트로웨팅 장치의 표면 평탄화 효과에 관한 연구

지도교수 김 희 찬

이 논문을 공학박사 학위논문으로 제출함

2013 년 8 월

서울대학교 대학원
협동과정 바이오엔지니어링 전공
이 충 희

이충희의 박사 학위논문을 인준함

2013 년 8 월

위 원 장 김 성 완 (인)

부위원장 김 희 찬 (인)

위 원 허 동 은 (인)

위 원 천 홍 구 (인)

위 원 주 세 경 (인)

Ph.D. Dissertation

A STUDY OF SURFACE POLISHING EFFECTS ON ELECTROWETTING DEVICES

BY

CHOONGHEE LEE

AUGUST 2013

INTERDISCIPLINARY PROGRAM FOR BIOENGINEERING
GRADUATE SCHOOL
SEOUL NATIONAL UNIVERSITY

A STUDY OF SURFACE POLISHING EFFECTS ON ELECTROWETTING DEVICES

BY

CHOONGHEE LEE

INTERDISCIPLINARY PROGRAM FOR BIOENGINEERING
GRADUATE SCHOOL
SEOUL NATIONAL UNIVERSITY

THIS DISSERTATION IS APPROVED FOR
THE DEGREE OF DOCTOR OF PHILOSOPHY

AUGUST 2013

DOCTORAL COMMITTEE :

Chairman _____ *Sungwan Kim, Ph.D.*

Vice Chairman _____ *Hee Chan Kim, Ph.D.*

Member _____ *Dongeun Huh, Ph.D.*

Member _____ *Honggu Chun, Ph.D.*

Member _____ *Segyeong Joo, Ph.D.*

Abstract

A STUDY OF SURFACE POLISHING EFFECTS ON ELECTROWETTING DEVICES

By

Choonghee Lee

Interdisciplinary Program for Bioengineering
Graduate School
Seoul National University

Driving force of droplet manipulation in electrowetting on dielectric (EWOD) device is an electric field. In all the EWOD devices, droplet is manipulated on surface, not in channel. Thus, surface roughness of the EWOD device aggravates droplet manipulation performance and reliability. In fabrication procedure, spacing between electrodes becomes a trench as deep as thickness of a metal deposition. The trenches increase surface roughness, resulting in increase of contact angle hysteresis (CAH) and decrease of

dielectric breakdown voltage.

In this dissertation, to resolve the problems created by trenches, chemical mechanical polishing (CMP) was applied before hydrophobic coating to remove trenches. By tilting plate method, it is experimentally verified that the CAH and tilting angle was increased with the number of trenches under droplet contact line. To verify that the polishing improves droplet manipulation performance and reliability, a unpolished and a polished EWOD device were fabricated. Droplet speed on the unpolished and the polished EWOD device were compared on three sizes of EWOD devices including 0.5 × 0.5, 1 × 1 and 1.5 × 1.5 mm^2 electrode array. Droplet speed of the polished EWOD device was improved by up to 100 %, from 35 mm/s to 70 mm/s with 3.5 μL droplet, compared with that of the unpolished one.

To clarify that EWOD device failure rate by dielectric breakdown is increased by strengthened electric field (E-field) on the trench edge, electric field intensity was simulated. With this simulation result, it was verified that E-field intensity on the trench edge of the unpolished EWOD device reduced by 42 % compared to that of the polished one. Also, dielectric breakdown voltage of the polished EWOD device was raised by 27 %, from 110 V to 140V, experimentally.

As well as droplet speed and device reliability, polishing trenches reduced heat generation of droplet. To verify this, an unpolished and a polished optoelectrowetting (OEW) device were fabricated. With parallel feeding 180 V of 100Hz AC sinusoidal signal to the

unpolished and the polished OEW device simultaneously, thermal image was acquired to compared temperature of 10 μL droplet mounted on the both devices. As a result, temperature difference between the droplet on the unpolished and the polished OEW device was 10 °C. Evaporation time of 1 μL droplet was measured with same setting with temperature difference experiment except for feeding voltage of 96 V ~ 192 V with 32 V spacing. Total evaporation time of 1 μL droplet on the polished OEW device was elongated by 92 % compared to that of the unpolished one in case of 192 V feeding. Dielectric breakdown voltage was also raised from 200 V to over 260 V.

Keywords: Electrowetting on dielectric (EWOD), Optoelectrowetting (OEW), Digital microfludics, Surface polishing, Contact angle hysteresis, Parallel bio-assay

Student Number : 2009-30954

CONTENTS

List of Figures

List of Tables

Chapter 1

1. Introduction

1.1 Electrowetting Platform as a Massive Parallel Bio-assay

Microfulidic total analysis system (μ-TAS) are specialized to detailed research topic [1-2]. To acquire specific results or satisfy own goal, many of constitutes consisting of μ-TAS are custom made for specific objective. Thus, μ-TAS are highly customized to specific application, resulting in narrow usage range, high cost to implement and labor-intensive. In addition, continuous flow based μ-TAS as shown in figure 1.1 (a) includes chip bonding procedure in fabrication for sealing. Several steps and skillful techniques are necessary for bonding procedure and it is obstacle for mass production of microfluidic chip. Also, for operation of microfluidic chip, most of them requires several pumping sources and valves that complexes

system configuration. In case of researches that requires parallel processing of sample, continuous flow based microfluidic device is not appropriate because of channel interference and complex tubing [1].

Thus, it is necessary to alternate complex microfluidic system with simplified operation mechanism and cost effective platform. In this regards, electrowetting is a powerful candidate to alternate continuous flow based microfluidic device because it employs electrical addressing as flow mechanism and does not require cover bonding procedure as shown in figure 1.1 (b). Because of electrical addressing, electrowetting based platform does not require pumping sources and valves and multi-droplet are manipulated individually by local activation for facilitate parallelism. In addition, droplet is manipulated on a flat surface of the electrowetting device, no channel patterning and sealing is required, resulting in simple fabrication. Fast droplet transport, maximally ~25 cm/s, is another powerful advantage of electrowetting based platform. Integration with other instrument for analysis is feasible because of no cover bonding [4].

In case of optoelectrowetting (OEW) platform, only two wiring to feeding device is required and droplet is manipulated by image pattern because of photoconductive layers switching E-field. Thus, OEW platform is appropriate for massive parallel bio-assay because implementing two wiring connection and image pattern manipulation let the OEW device far simple as shown in figure 1.2.

With these advantages, many researchers have endeavored to develop μ-TAS employing electrowetting device and various

application have invented biochemical reactors such as a DNA polyrase chain reaction [5], a bioassay [6], particle concentration [7] and cell seperation [8]. Thus, electrowetting technology is firmly positioned as a branch of μ-TAS.

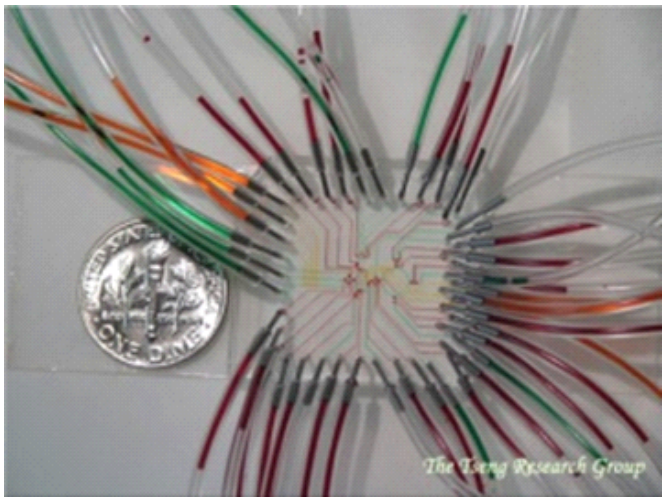

(a)

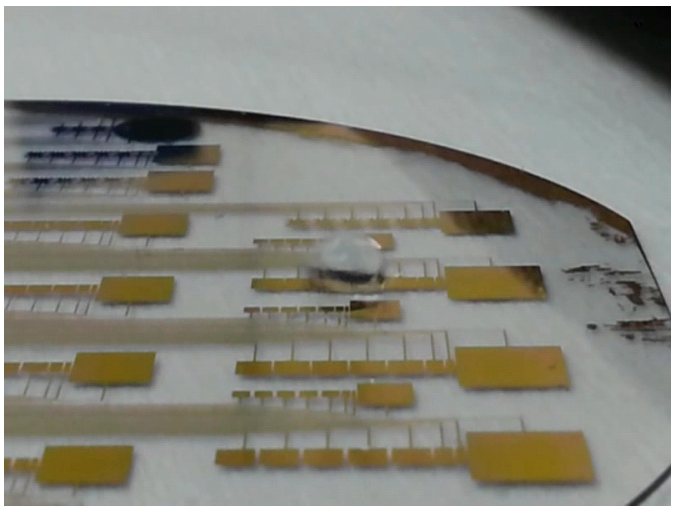

(b)

Figure 1.1 Comparison of configuration between channel-based microfluidic [1] and single plate EWOD device.

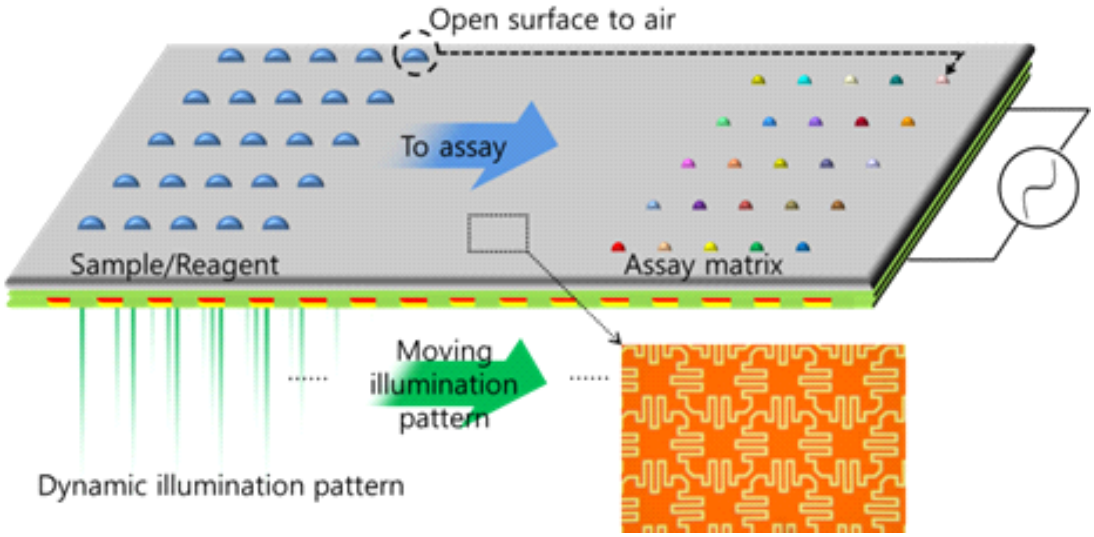

Figure 1.2 Open optoelectrowetting device for implementing massive parallel bio-assay.

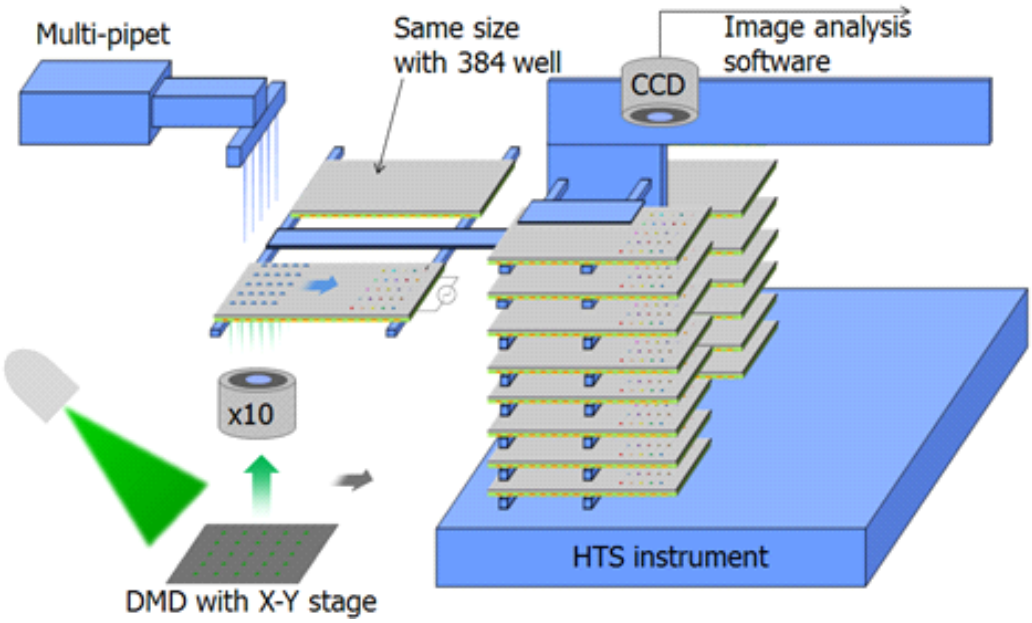

Figure 1.3 Example of conceptual diagram of massive parallel bio-assay using open optoelectrowetting platform shown in figure 1.2.

1.2 History of Electrowetting: By Configuration

Electrowetting on dielectric (EWOD) was firstly demonstrated by Dahms in the point of observed electrocapillary effect in 1969 [9]. At that time, he enlightened that it is possible to actuate liquid drop in capillary with electricity. In early 1990s, Berge illuminated that contact angle of a sessile drop on hydrophobic coated metal can be modulated by applying potential of several tens volt between grounded metal electrode plate and probe inserted to the drop [10]. In this experiment, the results were in agreement with electrowetting theory.

From Berge's EWOD demonstration, various trial to utilize EWOD technology have been done by many researchers. Washizu firstly demonstrated a single plate EWOD actuation of liquid droplets for micro-reactor application in 1998 [11] as in figure 1.1. The word "single" means all electrode to actuate droplet is included a substrate and a droplet is not sandwiched. He fabricated a micro-reactor, arrays of microelectrode covered with hydrophobic layer, and showed that micro-liter droplet can be transported, sorted and mixed with other droplet on that. With single plate device, droplet dispensing is feasible because of "open" configuration, no cover plate. Because of no cover plate characteristic, integration with other instruments such as optical detector, external sample reservoir and mass spectroscopy was feasible with single plate EWOD device. From Washizu, many researchers have tried to apply EWOD technology to microfluidic

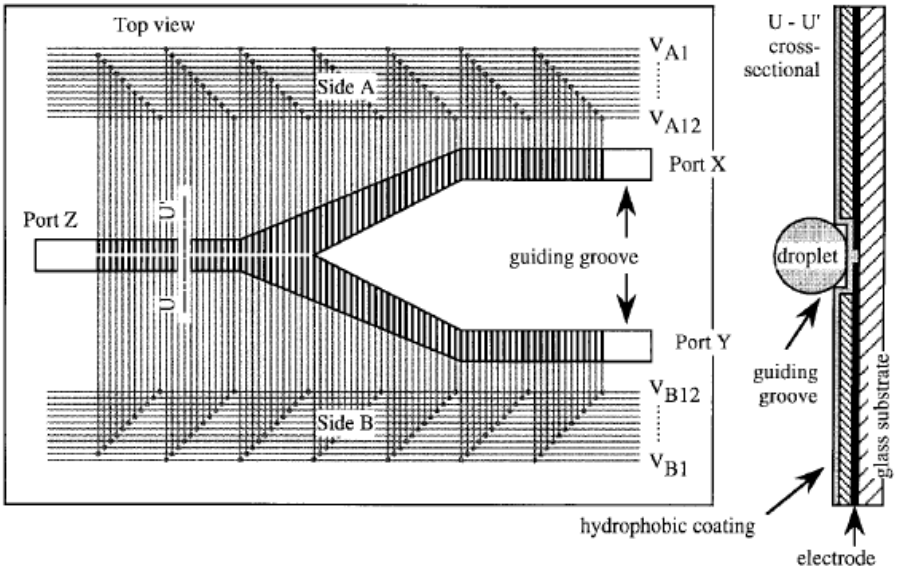

Figure 1.4 Schematic diagram of the first EWOD device success to droplet transportation, sorting and merging in 1998 by Wahshizu [11].

research such as biochemical analysis and development of research tool alternative to microfluidic chip. In 2000, Pollack at al. proposed a parallel plate (sandwiched configuration) EWOD device [12]. This configuration was comprised of a top and a bottom plate. The top plate consisted of a glass substrate, a ground electrode and a hydrophobic coating layer. On the top glass substrate, transparent Indium Tin Oxide (ITO) electrode was deposited to be grounded, and a hydrophobic layer was spin-coated for the two purpose of insulation and hydrophobic coating. On the bottom plate, ITO electrode was patterned to actuate droplet and the hydrophobic layer was deposited for the same purpose with the top plate. Parallel plate configuration introduced several advantages compared to Washizu's single plate configuration. First, because the droplet was squeezed by two plates, volume range to be handled by EWOD device was reduced to several hundred nano-liter level. This means if the EWOD device is utilized to biochemical reactor, cost to preparing sample can be reduced. Second, because the top plate provides more electromechanical force to actuate droplet than that of single plate device by introducing ground electrode, droplet manipulation is more feasible than in single plate device. Additionally, thin films are deposited or spin-coated over electrodes. This means that electrowetting devices are vulnerable to be damaged by high voltage actuation. In this regards, failure prone of the double plate EWOD device is reduced because potential than that of single plate device. Another advantage of double plate configuration is easy

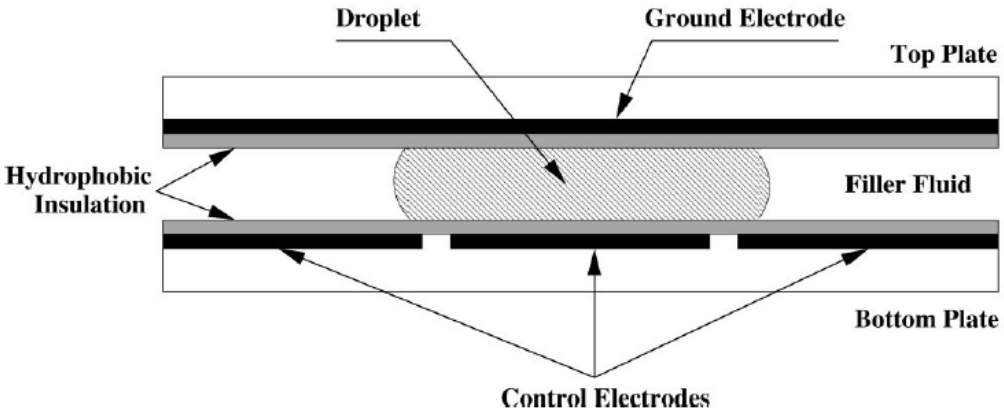

Figure 1.5 Double plate EWOD device developed by Pollack et al. in 2000 [12].

droplet splitting and extraction from reservoir because double plate device relatively exerts strong force on droplet. In electrowetting application, droplets necessarily are splitted and extracted from reservoir. These operations require relative high pulling force. Technical challenges of EWOD technology were as follow. First, available droplet range for each device was limited by size of electrode because diameter of the smallest droplet volume has to be larger than size of electrode. This is comprehensive that droplet is manipulated by fringing electric field. Second, if the number of electrode increases, too many electrical wirings complex device implementation and interfere precise droplet manipulation. For parallel observation or reaction of biochemical assay, EWOD technology is not appropriate. To resolve these problem, Chiou et al. proposed optoelectrowetting (OEW) device in figure 1.6 [13-14]. OEW device resolved interconnection problem of EWOD technology that complexes fabrication and implementation when parallelism increase by using photoconductive amorphous silicon layer. The photoconductive layer controls intensity of electric field that forces droplet by illumination of laser light and droplet transporting, splitting and merging were enabled. Still this OEW device utilized a pixelated electrode under amorphous silicon layer to generate electric field. This configuration limits droplet volume range like EWOD. Next, Chiou et al. reported continuous optoelectrowetting (COEW) device that alternate pixelated electrode with ITO electrode deposited evenly on a bottom substrate [15].

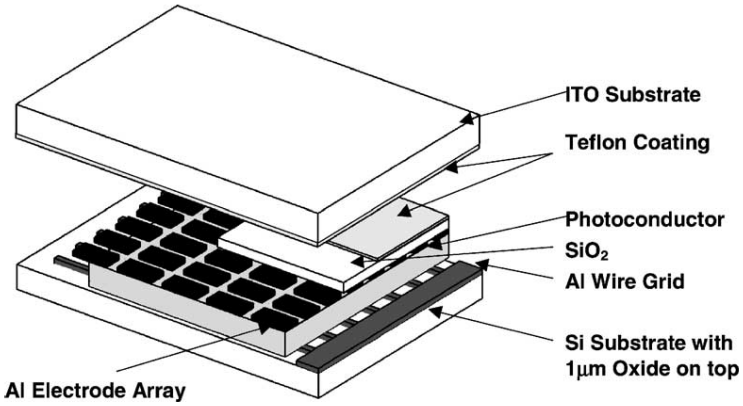

(a)

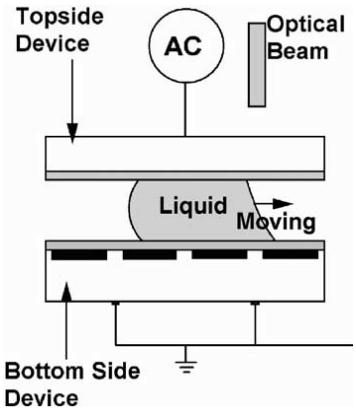

(b)

Figure 1.6 Schematic diagram of the first OEW device proposed by Chiou et al. (a) Layer composition and (b) simplified operation system [13].

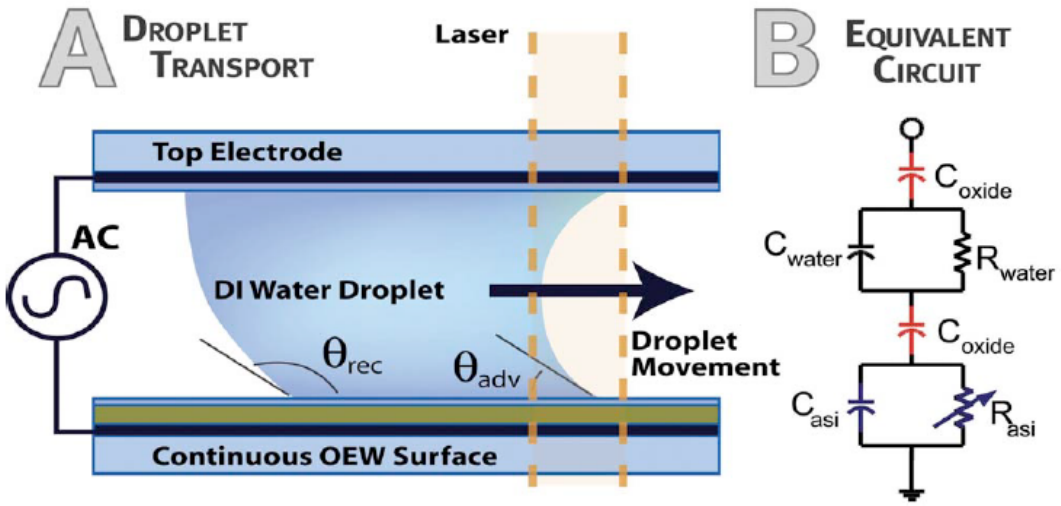

Figure 1.7 (a) Schematic diagram of the COEW device proposed by Chiou et al. (b) Electrical circuit mode [14].

Figure 1.7 shows the COEW device. Complex electrode wiring and resolution problems were avoided and pico-liter range droplet was successfully manipulated. They insisted that the optical illumnation on COEW device is “virtual electrode” because electric field was turned on the illuminated region on the device.

As in double plate EWOD structure, initial developed OEW and COEW device were implemented with double plate structure to utilize advantages of relative large electromechanical force to manipulate droplet compared single plate structure. However, droplet mounting on double plate devices is maximally 1-D as shown in figure 1.8 [16]. In this configuration, droplet dispensing require accurate alignment technique, needle array and augment dispenser. Considering that usual EWOD device is disposable, this access is not appropriate to parallel droplet manipulation.

In 2008, Chuang et al. developed open OEW (o-OEW) device, utilizing single plate OEW technique with pixelated electrode [17]. This configuration is appropriate to massive parallel bioassay because 2-D sample access is possible.

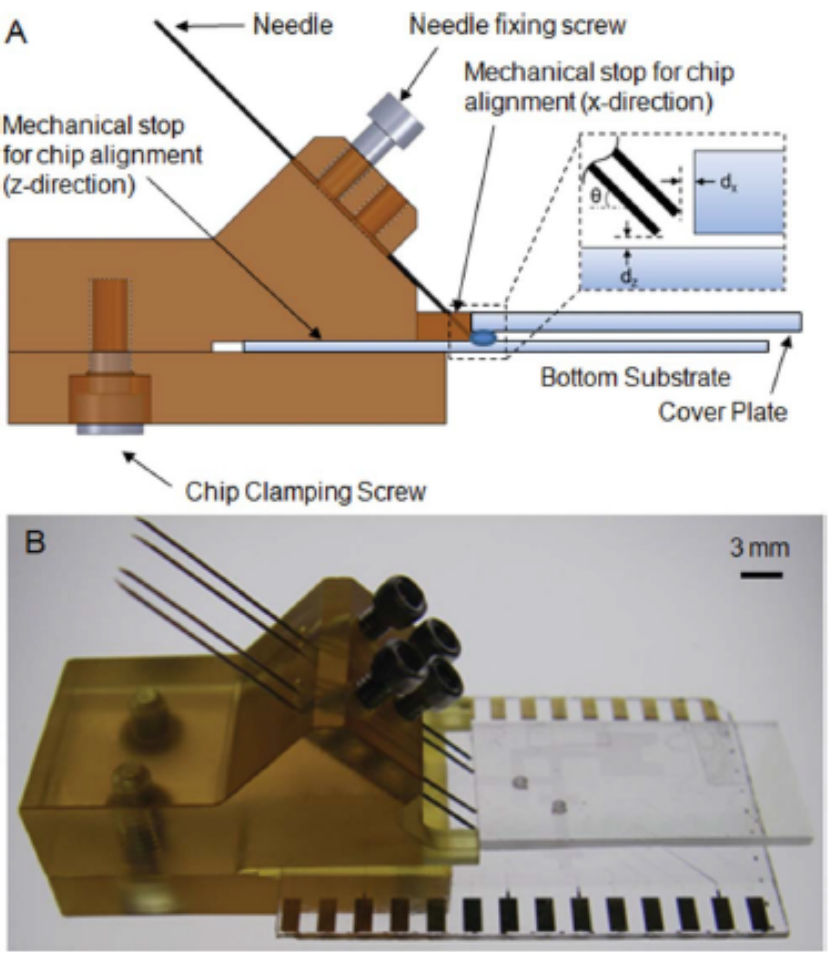

Figure 1.8 1-D droplet dispensing of double plate EWOD configuration. (a) Cross sectional view and (b) Image [16].

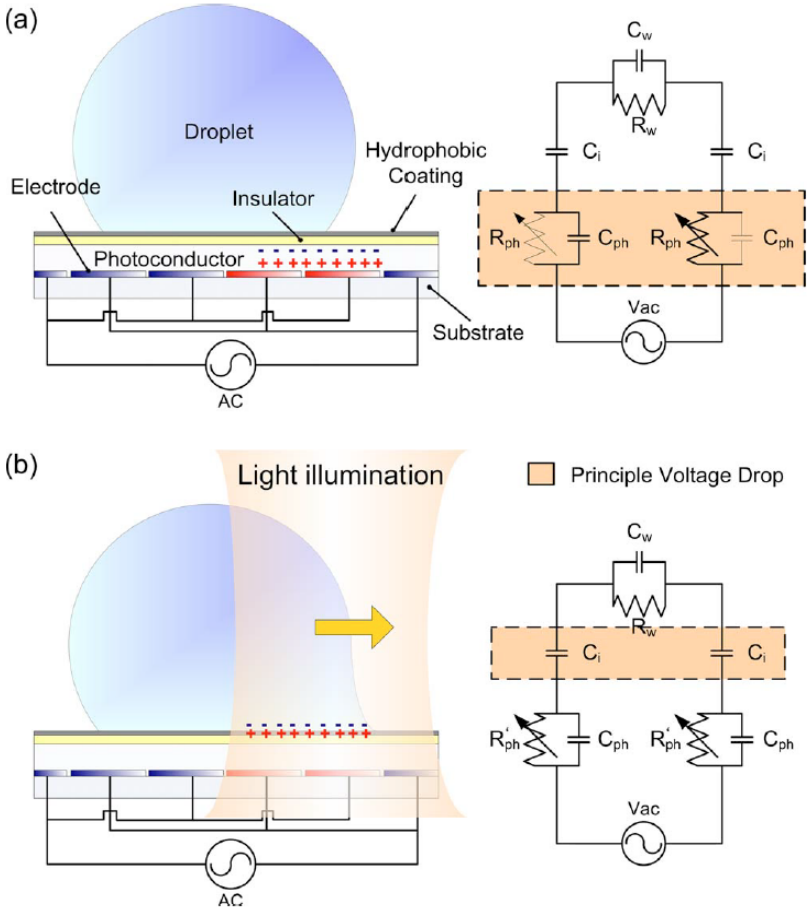

Figure 1. 9 Schematic diagram of the o-OEW device without laser illumination proposed by Chuang et al. [17] (b) When laser is illuminated, conductivity of photoconductive layer become is reduced to 4~5 order of magnitude and virtual electrode is formed.

1.3 Classification of Electrowetting Platform

The electrowetting device is classified to eight categories by three factors: manipulation mechanism, cover plate and medium. Manipulation mechanisms includes EWOD and OEW. When the electrode is activated in EWOD, E-field is generated and disappeared by turning off the activated electrode. That means droplet is manipulated directly turn on/off E-field. On the other hand, AC feeding potential is always applied to the all the two electrode of OEW Device. By illuminating photoconductive layer such as amorphous silicon, E-field is switched to the droplet.

By cover plate, electrowetting device are classified by double plate and single planar structure. In double plate device, droplet is sandwiched by both the top and bottom plate. Because of sandwiching, small volume of droplet under 1 μL can be used in the double plate EWOD device. Also, if a ground plate is included in the top plate, droplet pulling force is nearly doubled because electromechanical force is generated in two way. One is directed to the bottom electrode and the other is to the top. In single plate device, all the electrode is under insulating layer of the bottom plate. Advantages of the single planar electrowetting device are sample access and feasible implementation. Because the single planar device is open structure, droplet are mounted by pipetting in two dimension (2-D). It is important feature in case of parallel utilization. Without a cover plate, fabrication is easy.

Fluid medium, which are environment of operation, are silicone oil and air. With filling silicone oil, contact angle of droplet is increased to ~150°. This means that droplet manipulation become feasible because contact angle change is large with low voltage activation. However, using silicone oil for electrowetting device performing bio-assay due to reaction with samples. The air is appropriate for bio assay.

Table 1.1 show the summarized classified images of electrowetting devices by configuration and Table 1.2 include characteristics.

	EWOD		Optoelectrowetting (OEW)	
With cover (Double plate)	Oil 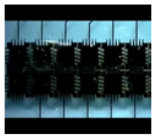	Air 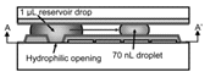	Oil (OET) 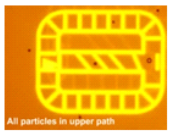	Air 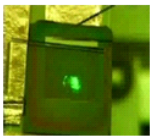
Open surface (single plate)	Oil	Air 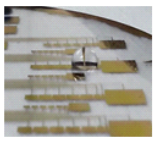 MELab (SNU) & DEPG (KU)	Oil 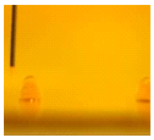	Air 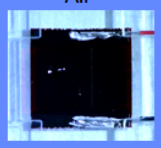 MELab (SNU) & DEPG (KU)

Table 1.1 Classification of electrowetting devices by manipulation mechanism, cover plate and fluid medium.

Cover plate	Media

• Double plate
  • Large contact angle hysteresis
  • 1-D sample access
  • Viscous lag
	• Immiscible media such as silicone oil
	  • Large contact angle hysteresis
	  • Contamination
	  • Sample access to substrate

• Single plate
  • 2-D sample access
  • Low contact angle hysteresis
	• Air (open surface)
	  • Easy sample mount
	  • Fast Evaporation

Table 1.2. Characteristic of OEW device by cover plate and media.

1.4 Technical Challenges and Research Objective

This study aims to investigating the effects of surface polishing on electrowetting devices. As mentioned before, many of electrowetting devices including various applications were implemented thanks to researchers endeavor. However, there are still problems to be overcome for commercializing and reliable usage.

For example, electrowetting devices are mainly failed by dielectric breakdown as figure 1.10 (a) and (b). Because electrowetting devices are necessarily operated by high voltage feeding to ~100V, strong electric field is generated between substrate and thin films as thick as total ~ 1 μm [18]. Additionally, compared to the strong dielectric strength of insulating layers such as silicon dioxide (SiO_2,1MV/cm) or silicon nitride (Si_3Ni_4, 1MV/cm), dielectric strength values of hydrophobic layers such as Teflon AF and CYTOP are as low as 21 kV/mm and 90 kV/mm, respectively [19-20]. This forces electrowetting devices disposable because device life time is short due to partial damage from dielectric breakdown. In addition, electrolysis is also another problem as shown in figure 1.10 (c). If insulating and hydrophobic layer are partially damaged, bubble are generated in the droplet.

Secondly, except for o-OEW devices, all the electrowetting devices include patterned metal under insulating layer. Inevitably, trenches as thick as metal electrode are generated on the surface, even after the edges of trenches than above the electrodes, the device failure

hydrophobic coating. These trenches increase the surface roughness, resulting in degradation of droplet speed and manipulation reliability of the devices as shown in figure 1.10 (d).

Third, heating is important issue if droplet volume becomes smaller than 1 μL. For example, 100 nL droplet is totally evaporated in 150 seconds following reference [21]. This means that if droplet is manipulated distance of 10 cm with the fastest open OEW device, speed of 3.6 mm/s, for 27 seconds, 27/150 of liquid in droplet is evaporated. Thus, heating generated by strong E-field near trench edges must be reduced because that accelerates evaporation of droplet.

To resolve these problems, the author investigated and verified that the trenches aggravate droplet manipulation performance and reliability of electrowetting device in figure A5. Then, applying polishing technique after insulating layer deposition helps to enhance maximum droplet speed enhancement and device reliability against to dielectric breakdown. Also, polishing was effective to reduce droplet heating. The summarized technical problems and solution are in Table 1.3

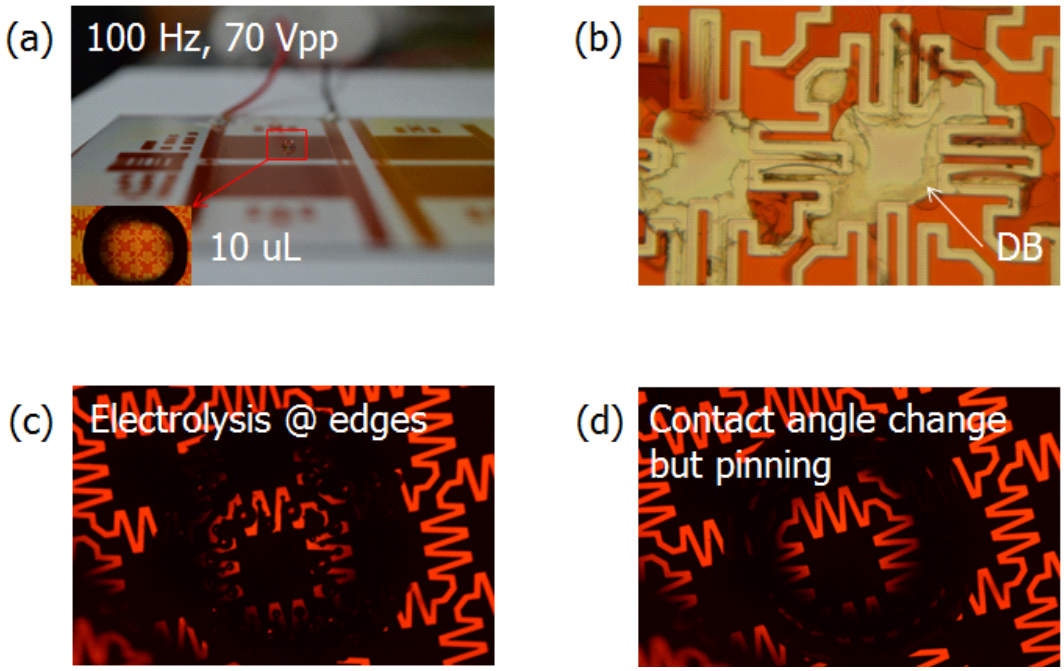

Figure 1.10 Problems related to trench edges in OEW device (a) experimental setting, (b) damage by dielectric breakdown, (c) electrolysis caused by partial damage or heating (d) droplet pinning.

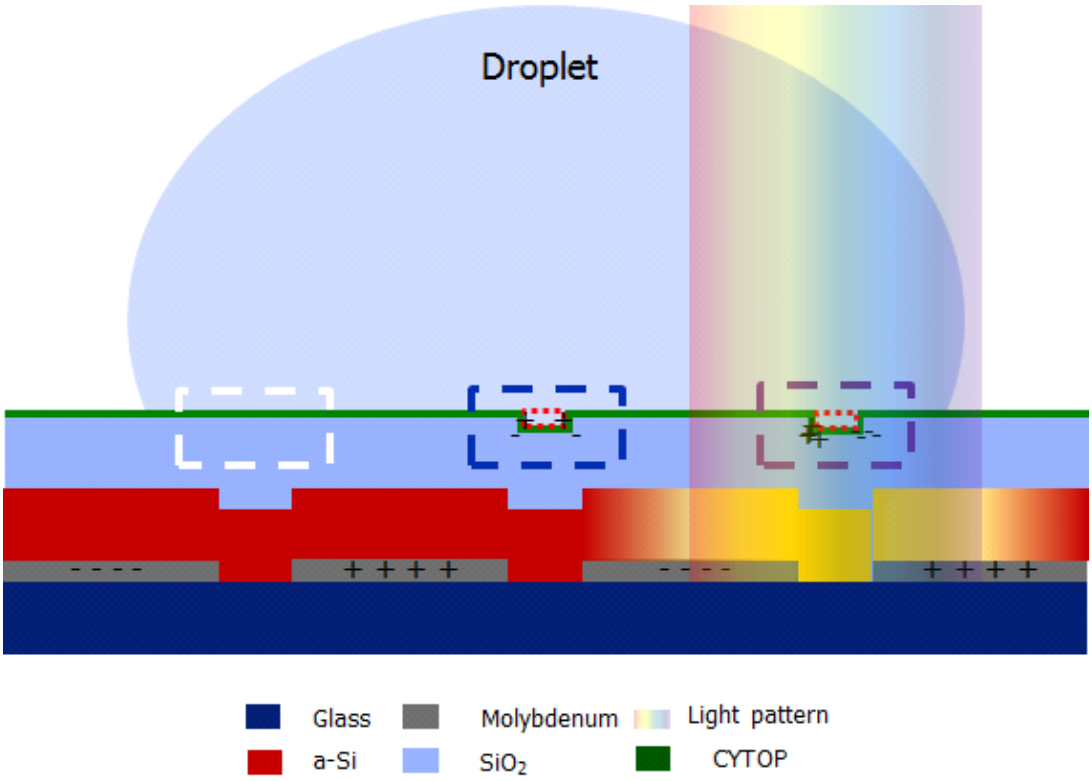

Figure 1.11 Schematic explaining hypothesis. Trench generated by electrode pattern and thin film depositions increases sourface roughness, resulting in interfacial area enlargement and unwanted E-field under droplet.

Technical challenges	Reearch Objective
• Droplet speed reduction & pinning	All these problems caused by surface trenches → Overcome by surface polishing 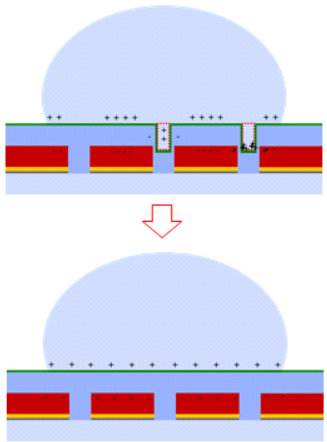

• Damage by dielectric breakdown
  • High potential (~100V)
  • Dielectric breakdown (< 0.5 um-thick)	

• Droplet fast heating • By high AC E-Field conduction via droplet	

Table 1.3 Summarized technical challenges and research objective.

Chapter 2

Surface Polishing Effect in Open EWOD Device

Droplet Speed Improvement and Device Reliability

2.1 Introduction

2.1.1 Theory of Electrowetting on Dielectric

Theoretical background of electrowetting is from Young-Lippmann Equation [20], which is,

$$\cos\theta_V = \cos\theta_0 + \frac{1}{2\gamma_{lv}}\frac{\epsilon_0\epsilon_r}{d}V^2 \qquad \text{(Equation 2.1)}$$

It describes the relationship between contact angle after applying

potential (θ_v), initial contact angle (θ_o), surface tension between liquid-vapor (γ_{lv}), relative permittivity (ε_r) and applied potential (V). However, the Equation 2.1 fits on limited range because it came from dynamics of a sessile drop as shown in figure 2.1. Thus, in case of moving droplet, many researchers tried to find the precise dynamics of droplet, but the debates are not ended. Alternatively, in this dissertation, mechanics of droplet movement is descripted in qualitatively with the figure 2.2. First, the droplet are mounted on surface of the EWOD device with high contact angle over 115° and potential is applied to the center electrode. Second, strong electric field is generated via thin film ($<$ 1 um) including the insulating and hydrophobic layer. Third, because of this strong electric field, the liquid and the thin films are polarized. Fourth, the polarized charges are condensed on contact line by the lightning rod effect. In this situation, the electric field intensity on the contact line is very strong, resulting in pulling the contact line to the direction of the activated electrode. Fifth, by the pulling force, the shape of the droplet is changed and the contact angle is reduced. With this transformation, internal pressure by surface tention is unbalanced and the hydrodynamic force are generated. Sixth, with the electrodynamic and hydrodynamic force, the droplet is moved to the direction of the activated electrode.

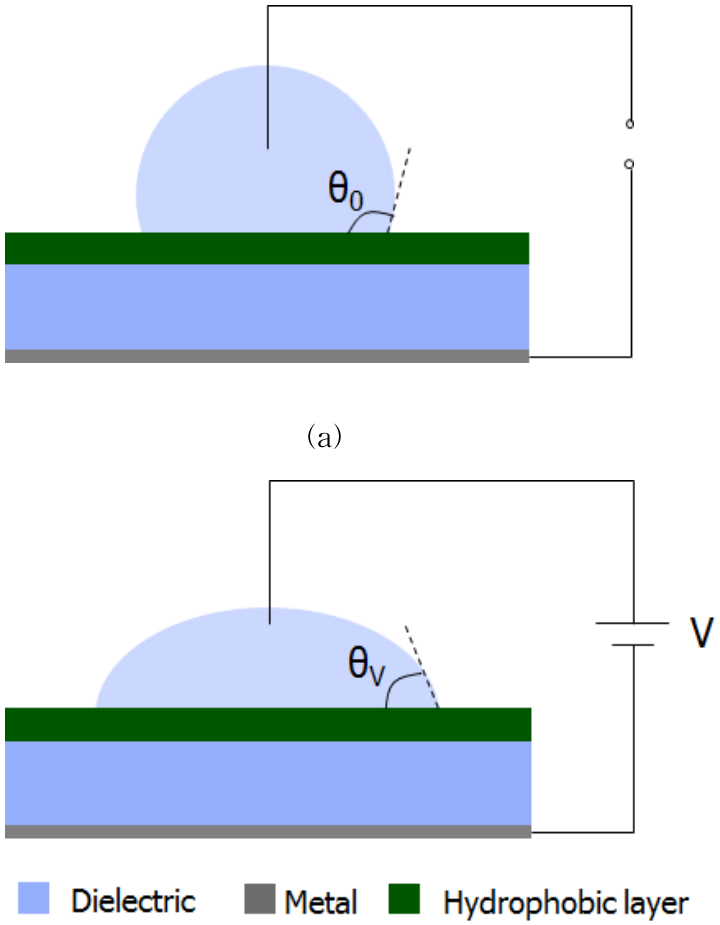

Figure 2.1 The schematic of the electrowetting experiment. (a) Potential is not applied to the sessile drop. (b) When potential V is applied to the sessile drop, the contact angle in triple contact line is reduced with the tendency of Young-Lippmann equation.

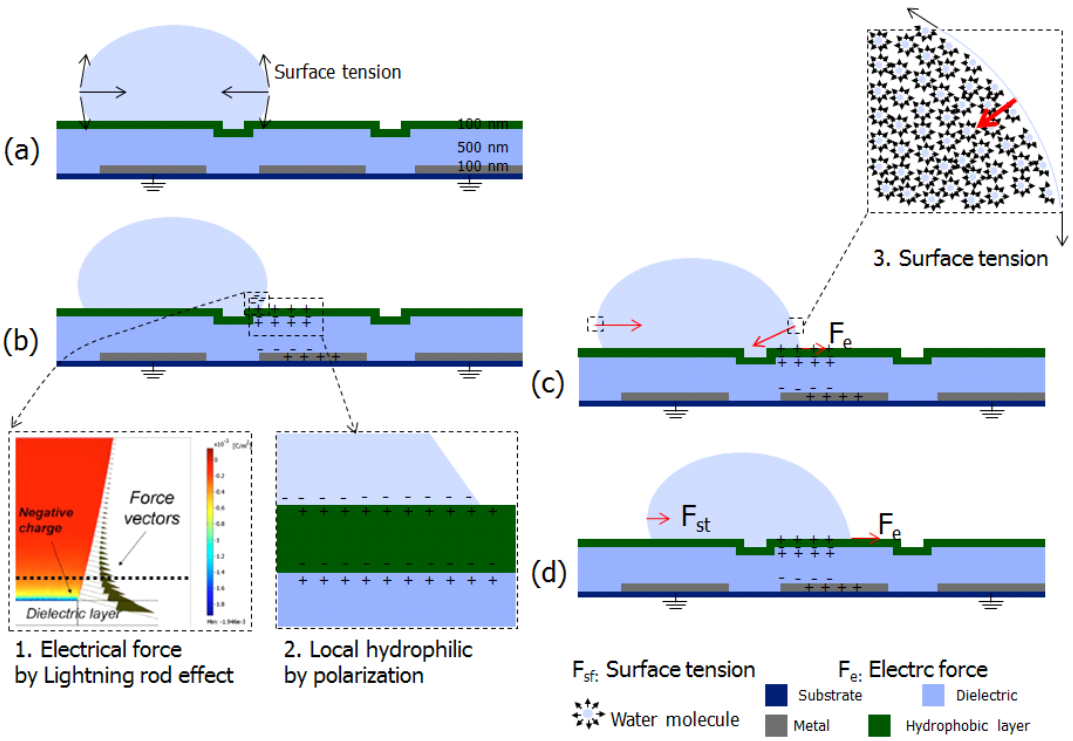

Figure 2.2 Sequential schematic diagrams that explain the procedures of droplet movement.

2.1.2 Chemical Mechanical Polishing

Chemical mechanical polishing (CMP) is the necessary process of planarization in semiconductor fabrication [20]. The CMP instrument consists of a wafer mounting head, a slurry and a polishing head. During CMP process the wafer is fixed on the rotating mounting head. The slurry including deionized water, abrasive and etchant is sprinkled by a nozzle and distributed by a conditioner on the rotating polishing head. By pressing the rotating wafer mount against the rorating polishing head, the wafer is grinded with ~100 nm/min rate [20]. On the surface of the wafer, mechanical wearing and chemical reaction is simultaneously, resulting in the planarization of the wafer. The figure 2.3 shows the configuration of CMP instrument.

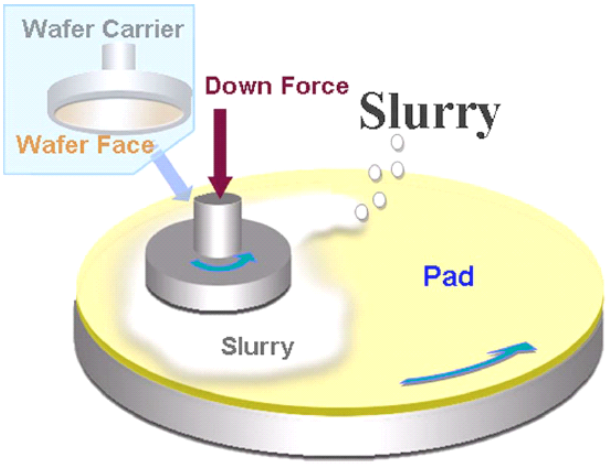

Figure 2.3 Schematic diagram of CMP instrument [20]. It includes the slurry, the rotating wafer mount and polishing pad. Chemical reaction and mechanical friction with the abrasive in slurry cause the wafer surface grinded.

2.1.3 Goal of This Study

The important competitiveness of EWOD compared to other miniaturized chemical analysis technologies like continuous microfluidics is to manipulate sample droplets fast with electrical addressing [1]. Thus, EWOD does not require external pumping sources that complex system configuration for manipulating droplets. This enables EWOD true miniaturized and portable implement. Also, EWOD system features various advances such reconfigurability for customizing to specific objective and low cost fabrication for disposable use [21-26].

In EWOD system, droplets including samples and reagents are manipulated with electric field generated by the potential applied between electrodes [27-28]. Young-Lippmann equation in (2. 1) describes the macroscopic physics among contact angle, applied electrical energy and surface tension. Figure 2.4 shows the schematic of single planar EWOD configuration. By applying several tens or more strong volts between electrodes, contact angle of droplet on the activated electrode side is reduced by the mechanism of equation (2. 1), resulting in internal pressure unbalance of droplet. This unbalanced pressure difference is driving force of droplet.

In real world application, because the surface of the EWOD device is not perfectly planar and has adhesion force by physical heterogeneity with droplet, high voltage over a threshold potential, minimum potential difference to move droplet above another electrode,

is required. In addition, defects and irregularity on the surface of the EWOD device can exist because of several thin film deposition and spin-coating necessary to fabrication process of EWOD device. Residues attached from air in fabrication process and impurities in droplet also aggravate the droplet manipulation in the EWOD system [29]. All these inherent technical challenges causing random pinning force between droplet and the surface of the EWOD device increases contact angle hysteresis [30-33].

For fabrication of the EWOD electrodes, a metal thin film layer is deposited and patterned on a substrate. Then, insulating layer is deposited by chemical vapour deposition, follows by spin-coating of hydrophobic layer. In these processes, trenches as deep as metal electrodes are remained on the surface of the EWOD device, resulting in irregular surface as shown in figure 2.1. The trenches impede reliable droplet manipulation as follow [34]. First, the trench increases surface roughness of EWOD device. This causes random pinning force and contact angle hysteresis increase, resulting in increasing threshold potential [35-36]. Second, on the trench edge, electrolysis by dielectric breakdown is more easily generated because of imperfect step coverage as shown in red dotted box of figure 2.4 Because strong electric field by high potential is applied between electrodes, thin films on the trench walls are vulnerable to be damaged by dielectric breakdown. Electrolysis of droplet by dielectric breakdown mainly causes EWOD device failure. Especially, dielectric strength of hydrophobic coating material such as Teflon AF 1600 or CYTOP is

weak as 21 and 91 kV/mm, respectively, and usually, deposited thickness is 50 ~ 200 nm. These coating is destructed first before relatively thick insulating layer such as silicon dioxide, silicon nitride or parylene [37].

We investigated the relationship between the number of trenches and CAH, and the effect of removing the trenches on droplet manipulation performance of EWOD device on droplet manipulation performance improvement. To verify that trenches increase CAH, we measured it on various electrode width and pitch by tilting plate method. Then, droplet manipulation performance was investigated by comparing unpolished single planar EWOD device with one that was removed trench and polished by CMP. The CMP was effective additional process for enhancing droplet speed and preventing electrolysis by early dielectric breakdown, resulting in reliable operation.

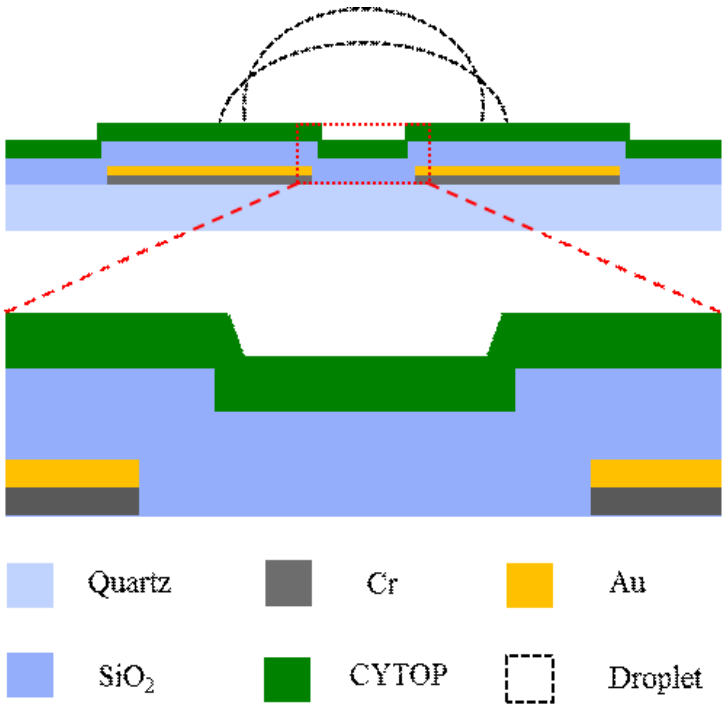

Figure 2.4 Schematic of unpolished EWOD device and magnified trench between electrodes.

2.2 Experimental Section

2.3.1 Electric Field Intensity Simulation near Trench

On the trenches of the unpolished EWOD device, the droplet was pinned and speed of that was reduced. Also, the fact that electrolysis was mainly created near trench edge means there was device damage by DB. For verifying that the cause of droplet speed reduction, pinning and device failure by DB, it is required to observe the electric field intensity distribution, especially near trench. The simulation was fulfilled in two dimensional in COMSOL 4.0. Figure 2.5 shows the simulated geometry. For simplicity and convergence of simulation, width of the electrode and spacing was reduced to 5 um and 3um, respectively. Vertical dimension (100 nm-thick electrodes, 500 nm of insulating and 100 nm-thick hydrophobic layer) was not changed because it is important to approximate the calculated E-Field intensity to the real situation. 100 V of 100 Hz was applied the eledtrode on the right of the center and the other was grounded. Figure 2.6 shows the entire view of the simulation result including equipotential line and E-field intensity distribution. As expected from the results of experiment, E-field was strong near the activated electrode. Figure 2.7 includes the magnified views of the white-dotted box in figure 2.6. In the unpolished case, the E-field intensity on the

corner of the trench was ~252 V/um, where that of the polished was ~146 V/m. Because of imperfect step coverage, insulating layer deposition is nearly zero near the wall of the trench. This case is the worst case. Thus, the 3 case was simulated by step coverage in the range that the trench edge can be. The result of these 3 simulation is shown in figure 2.7. In case of the edge of electrode, all the results were similar with 400 V/um of E-field intensity. However, in case of the U and P position, E-field intensity was reduced by 41 %, from 252 V/um to 146 V/um. Thus, the strengthen E-field on trench edge is the cause of droplet speed reduction, pinning and early DB. Also, it is suspected that strengthened E-field is one of main cause of droplet pinning because the E-field on the trench edge could generate interfering force of droplet movement.

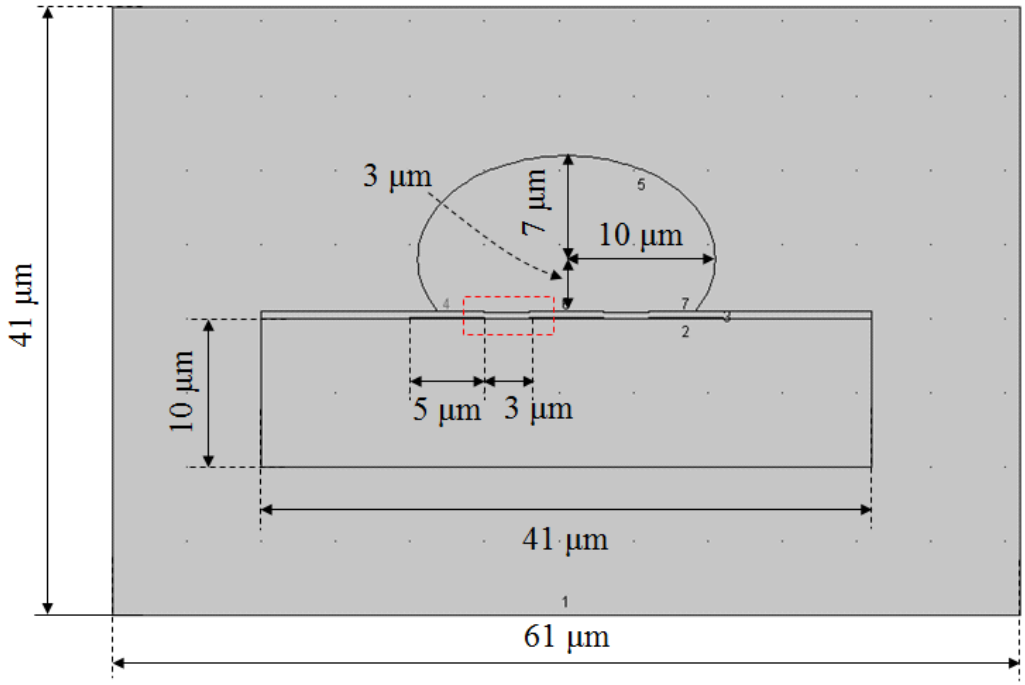

(a)

(b)

Figure 2.5 The dimensions of the simulated geometry. (a) The entire view. (b) The magnified view of the red-dotted box in (a).

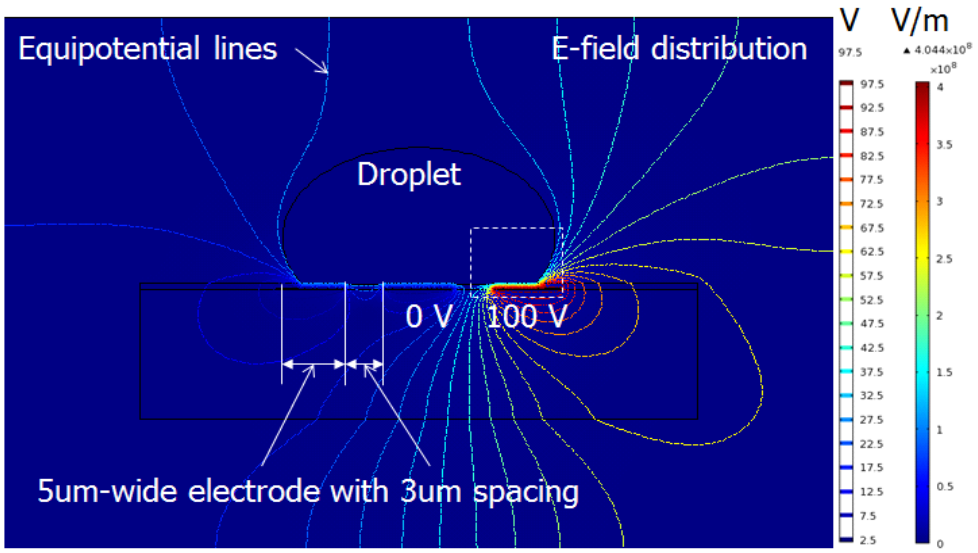

Figure 2.6 Simulation results with equipotential line and E-field distribution.

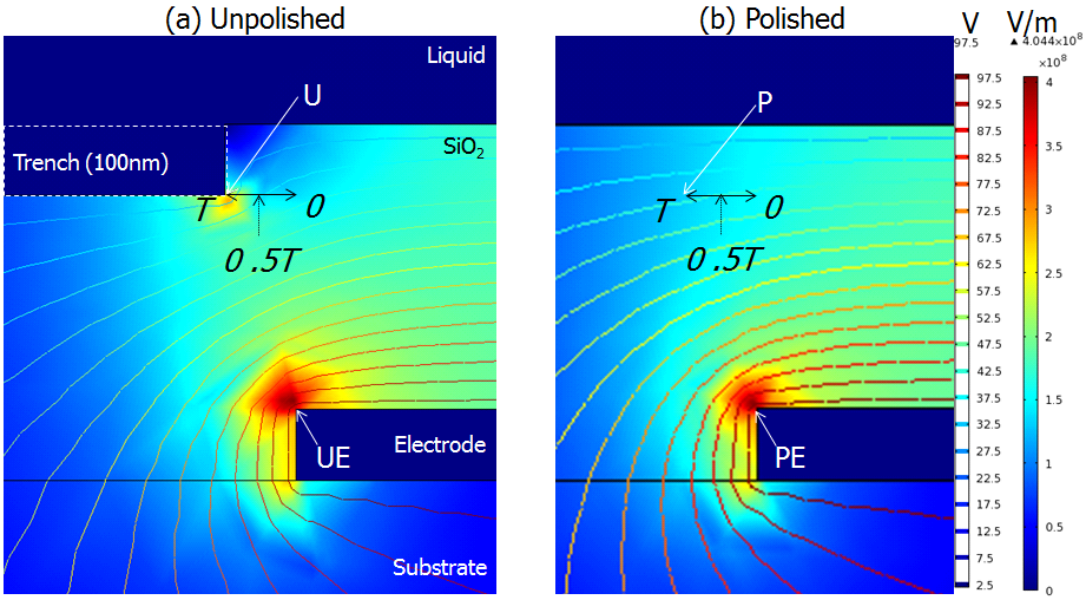

(a) (b)

Figure 2.7 The magnified view of the white-dotted box in the figure 2.19. (a) The unpolished and (b) the polished device.

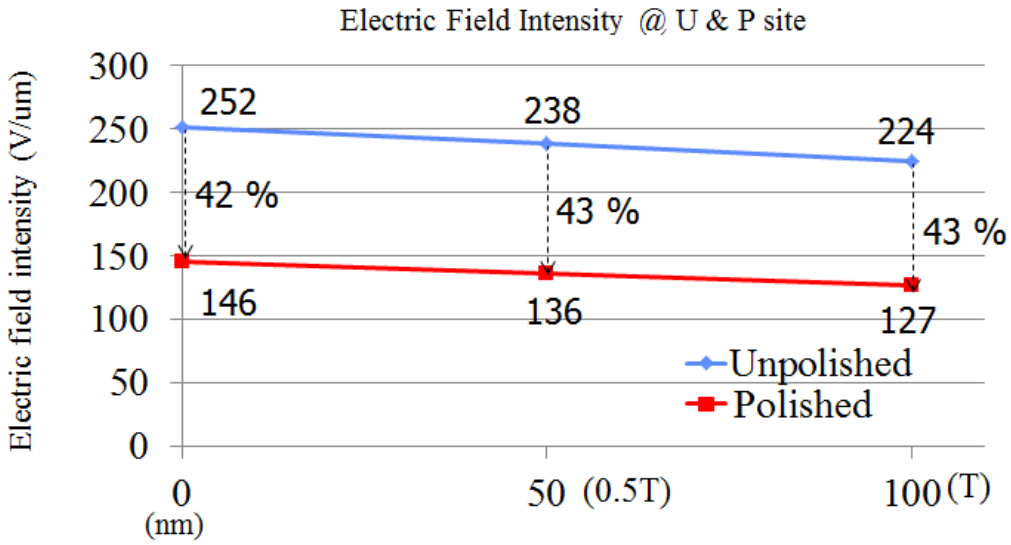

Figure 2.8 Comparison of the E-field intensity in the unpolished and the polished EWOD device.

2.2.2 Modeling

Determining the thickness of the insulating and hydrophobic layer is important because they determine the electric field intensity. This means that the driving force of the droplet and dielectric breakdown voltage are limited by the thickness of the insulating and hydrophobic layer. Following the Young-Lippmann equation, if the thickness of the insulating and the hydrophobic layer becomes thin, the droplet driving force becomes larger, but dielectric breakdown voltage becomes smaller. Because of this compromise, the thickness of the insulating and hydrophobic layer should be in a range which enable droplet transport with sufficient force and high dielectric breakdown voltage for reliability.

In this regards, mathematical parameter modeling including the thickness of the insulating and hydrophobic layer, contact angle, potential and permittivity was done with the Matlab, based on the Young-Lippmann equation. The figure 2.9 show the simplified schematic model of the EWOD device. For droplet transport, minimum contact angle change should be over 30° [22]. Also electrowetting number, which are the second term in the right of the Young-Lippmann equation, should be maximized for robust droplet movement. To acquire contact angle change over 30° and avoid high electric field over dielectric strength of hydrophobic layer. The modeling was focused on to find maximum electrowetting number with variation of the thickness of the insulating and the hydrophobic

layer in the equations from (2.2) to (2.4).

For given potential, the electric field variation with the thickness of the insulating and the hydrophobic layer was calculated based on the equations from (2.2) to (2.4) as in figure 2.10. With this result, the thickness range that does not damage the hydrophobic layer was found under 90 V/um of the dielectric strength of the hydrophobic layer (CYTOP). Next, the thickness range enabling the EWN over 35° was found as in figure 2.12. With these results, the thickness of the insulating and the hydrophobic layer were determined as 500 nm and 100 nm, respectively.

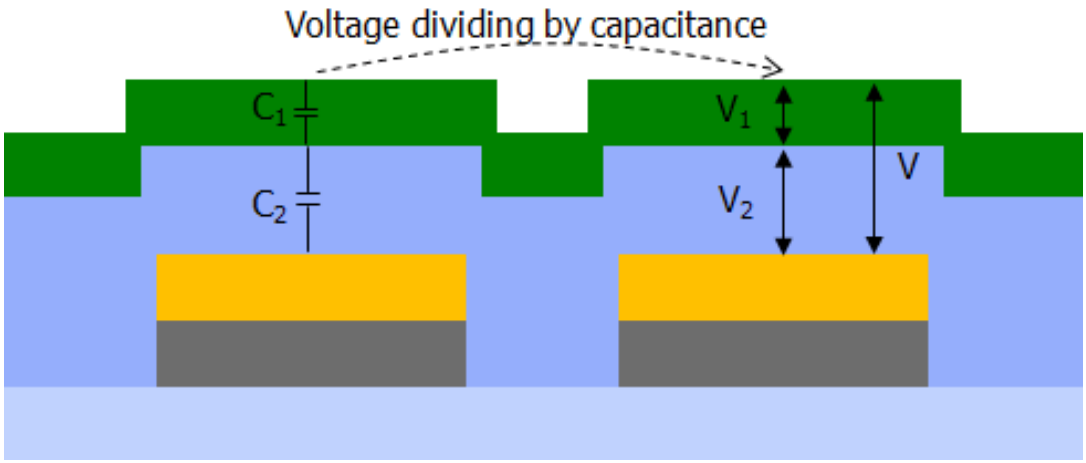

Figure 2.9 Schematic model of the EWOD device for determining of the parameters of the Young-Lippmann equation.

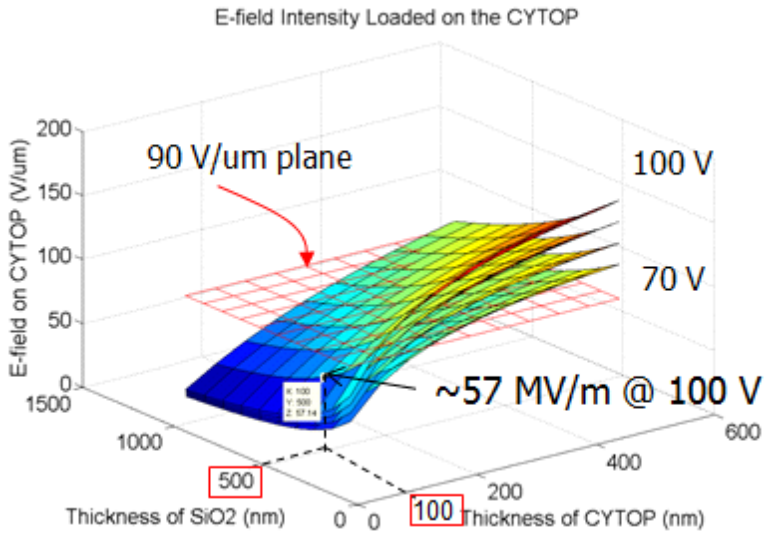

Figure 2.10 Two dimensional surface diagram of the E-field intensity loaded. on the hydrophoboc layer (CYTOP).

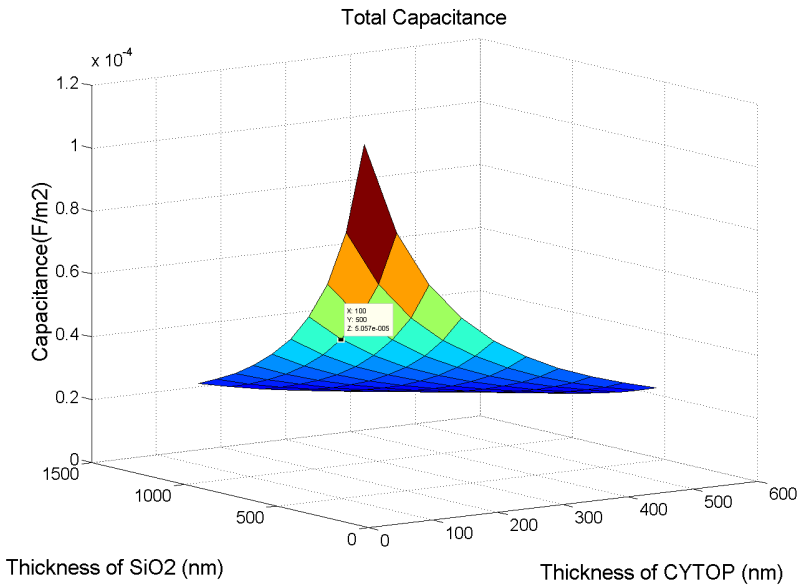

Figure 2.11 Two dimensional surface diagram of total capacitance by combination of silicon dioxide and CYTOP layer thickness.

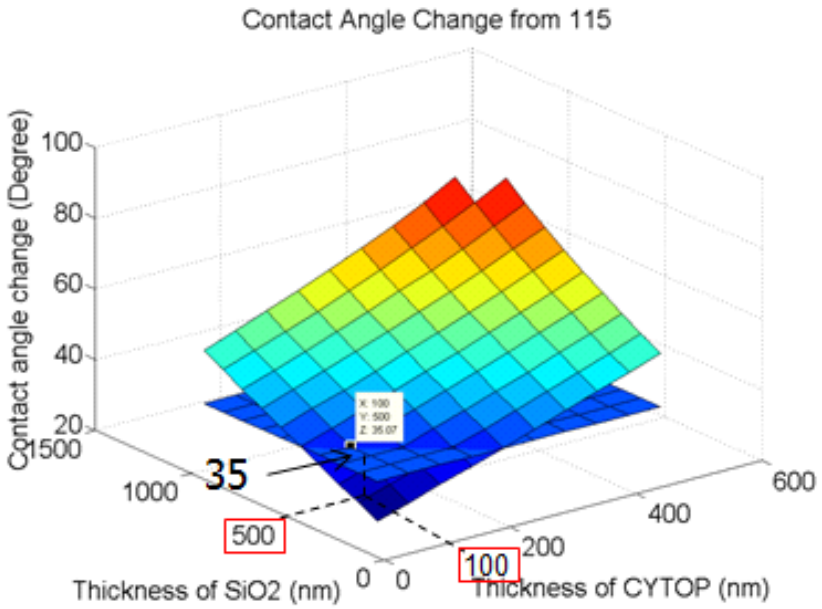

Figure 2.12 Two dimensional surface diagram of contact angle change for finding contact angle change over 35°.

$$EWN = \frac{1}{2\gamma} C_{tot} V^2 \text{ where } C_{total} = \frac{C_1 C_2}{C_1 + C_2} = \frac{\varepsilon_1 \varepsilon_2}{\varepsilon_1 d_2 + \varepsilon_2 d_1} \quad \text{(Equation 2.2)}$$

$(1 : CYTOP, 2 : SiO_2)$

$$V_{max} = V_{max1} + V_2 \quad \text{(Equation 2.2)}$$

$$V_{max1} = E_{max1} \times d_1 = \frac{\varepsilon_2 d_1}{\varepsilon_1 d_2 + \varepsilon_2 d_1} V_{max} \quad (E_{max1} = 90V / um)$$

(Equation 2.3)

$$EWN_{max} = \frac{1}{2\gamma} \frac{\varepsilon_1 \varepsilon_2}{\varepsilon_1 d_2 + \varepsilon_2 d_1} \times (E_{max1} \times d_1 \times \frac{\varepsilon_1 d_2 + \varepsilon_2 d_1}{\varepsilon_2 d_1})^2$$

$$= \frac{1}{2\gamma} {E_{max1}}^2 \times \frac{\varepsilon_1}{\varepsilon_2} \times (\varepsilon_1 d_2 + \varepsilon_2 d_1)$$

(Equation 2.3)

2.2.3 Mask Design

Figure 2.13 shows the mask design for the unpolished and the polished EWOD device. It consists of three kinds of schematic for testing wide range of droplet volume. 0.5×0.5 mm^2 with 25 μm for 1 ~ 2.5 μL, 1×1 mm^2 with 50 μm for 3.5 ~ 5 μL, and 1.5×1.5 mm^2 electrodes 100 μm spacing for 7.5 ~ 10 μL range of droplet volume, respectively. The mask was designed with the Cadence Virtuoso. Because minimum spacing between electrodes was 25 μm in this mask, it was printed on transparent film.

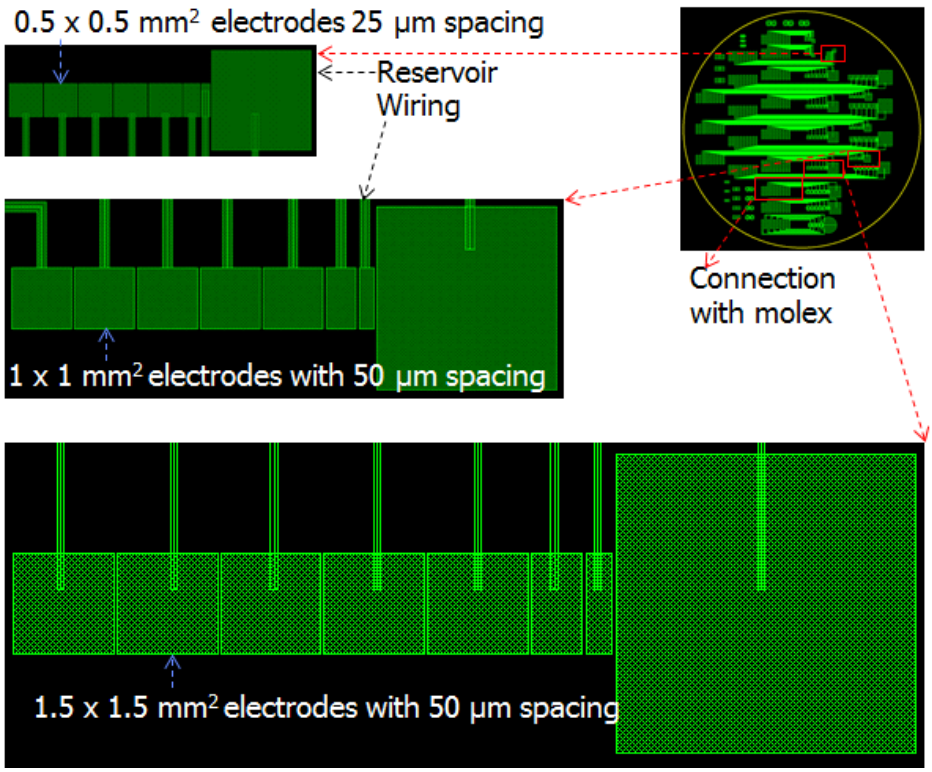

Figure 2.13 Mask design for the unpolished and the polished EWOD device fabrication.

2.2.4 Fabrication

2.2.4.1 Interdigitated Electrodes for Contact Angle Hysteresis Measurement

To investigate whether the number of the trenches increases CAH, devices including interdigitated electrodes with various width and spacing were fabricated. Figure 2.14 shows fabrication process. On square glass substrate, 50 nm-thick Molybdenum layer was deposited, followed by standard photolithography to pattern electrodes by wet-etching. As insulating layer, 0.9 um-thick silicon dioxide was deposited using plasma enhanced chemical vapour deposition (PECVD) (Model 310PC, STS Ltd., Wales, UK). CYTOP (CTL-809M, Asahi Glass Co., Ltd, Tokyo, Japan) diluted to 1 % with amorphous fluoropolymer solvent (FC-40, 3M, MN, USA) was spin-coated with 1000 rpm, resulting in 100 nm thick. CAH was measured on the devices using tilting plate method.14 It was fixed on a chuck of a fully automated CAH measuring instrument (SmartDrop, femtofab, Korea), which utilizes tilting plate methods, as shown in figure 2.9. A 10 μL droplet was mounted on the device in vertical direction with respect to the direction of the interdigitated electrode fingers. The plate and camera rotates with 0.76°/s, followed by image processing for calculating CAH. Surface profile was attained by using stylus surface profiler (Alpha-Step D-100, KLA-Tencor, CA, USA) with stylus probe speed of 80μm/s.

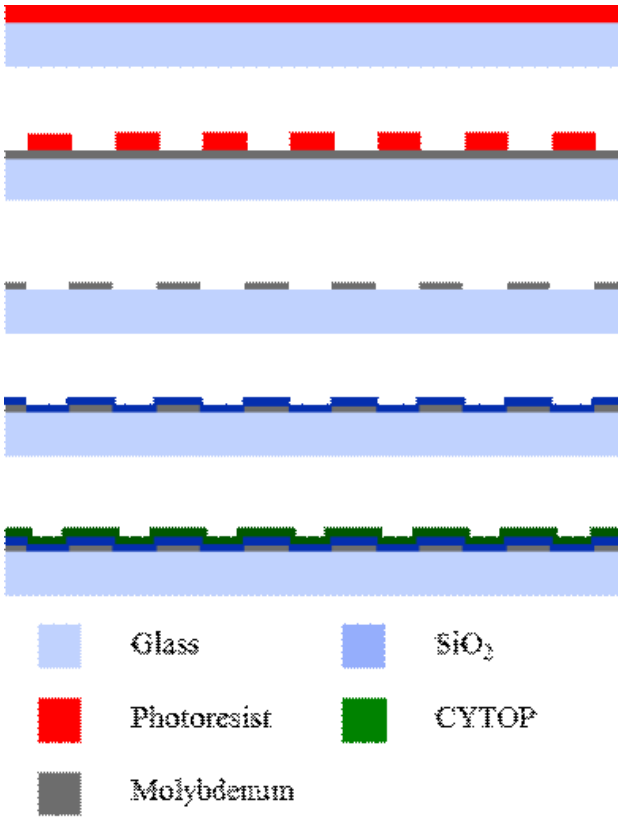

Figure 2.14 Fabrication procedure of the contact angle hysteresis variation test device.

2.2.4.2 A Unpolished and a Polished EWOD device

To compare droplet manipulation performance between polished EWOD device by CMP and unpolished one, both EWOD devices were fabricated as shown in figure 2.15 (a) and (b). For fabricating electrodes, negative photoresist (AZ-5214E, Clariant, Switzerland) was patterned on quartz wafer, using standard photolithography for lift off. Cr(20nm)/Au(100nm) layer was deposited by ebeam evaporator (ZZS550-2/D, Maestech co., Ltd, Korea), followed by lift off. Then, 500 nm-thick silicon dioxide layer was deposited by PECVD, and 100 nm-thick CYTOP was spin-coated. In case of the polished EWOD device, 700 nm-thick silicon dioxide was deposited and the upper 200 nm-thick surface including trenches was polished by CMP instrument (Poli 500 R&D CMP, G&P Technology, Korea). Then, 100 nm-thick CYTOP was spin-coated. For observing to manipulate various droplet volume range, 0.5 x 0.5, 1 x 1, 1.5 x 1.5 mm2 electrode arrays with 25, 50 and 100 μm spacing were prepared, respectively.

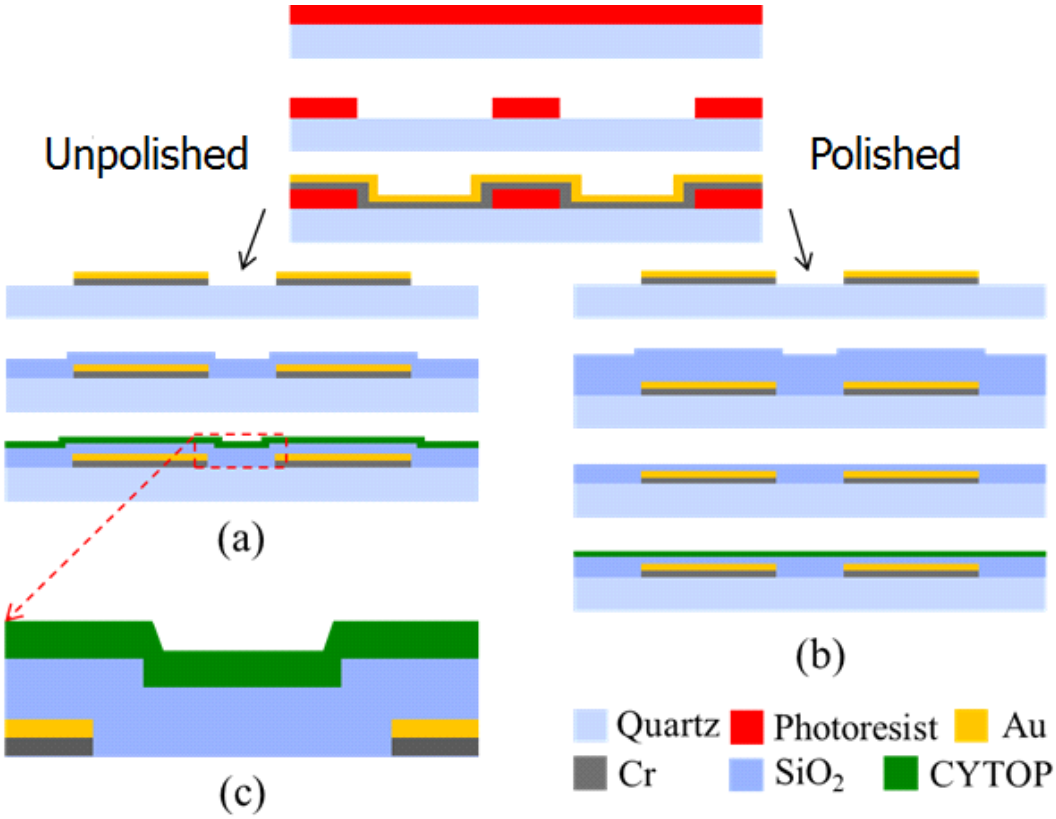

Figure 2.15 Fabrication process of (a) the polished EWOD and (b) the unpolished EWOD device

2.2.5 Experimental Setup

2.2.5.1 Contact Angle Hysteresis Measurement

Contact Angle Hysteresis was measured by tilting plate method [30] using SmartDrop (femtofab, Korea) shown in figure 2.16. After mounting the hydrophobic-coated interdigitated electrodes, 10 μL droplet was dispensed on that. When measurement starts, the chuck in the SmartDrop rotates with 0.1 °/s speed and acquires image of the droplet. The image was analyzed by bundle software with 0.1 ° precision

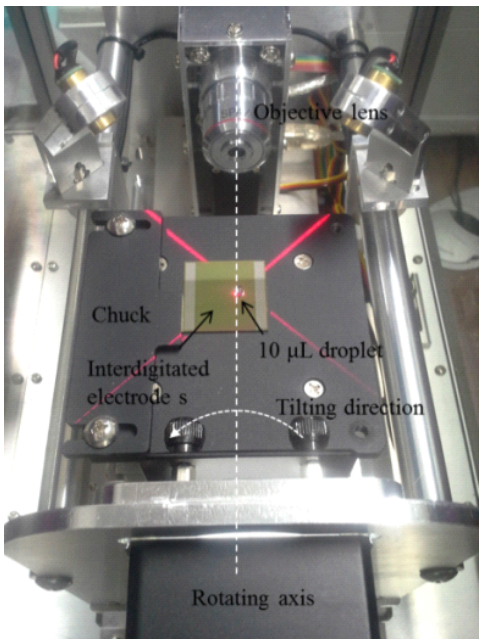

Figure 2.16 Measurement setup of CAH variation test using the tilting plate method.

2.2.5.2 Droplet Speed and Breakdown Voltage Measurement

Figure 2.17 shows schematic of EWOD operation system. To activate EWOD devices, a digital DC power supply, in-house high voltage amplifier and relay array (DS1E-S-DC5V, Panasonic, Japan) were used. The relay array control software was programmed with LabVIEW language (National Instrument, TX, USA).

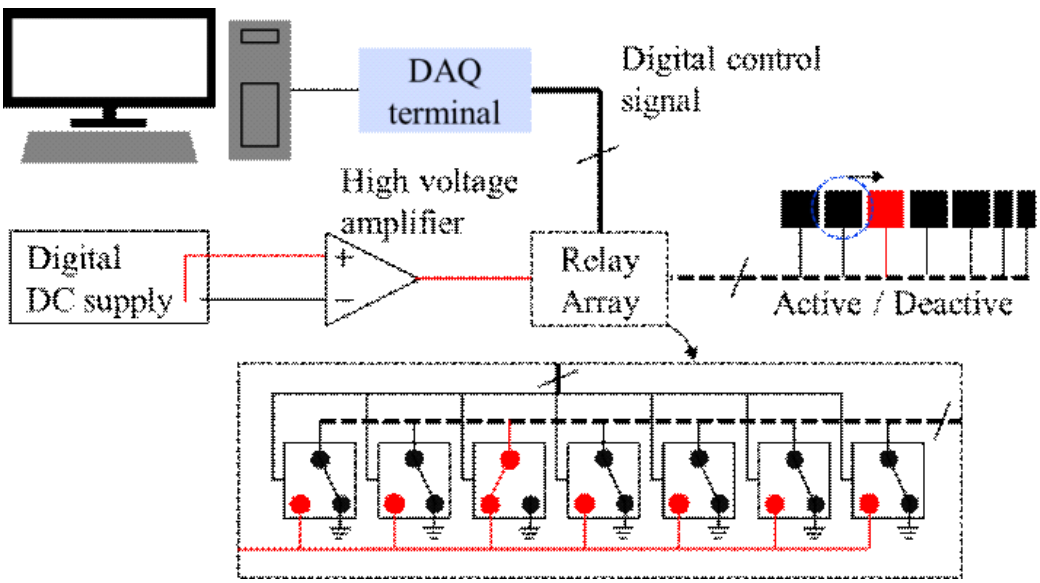

Figure 2.17 Schematic of EWOD operation system configuration

2.3 Results and Discussion

2.3.1 Contact Angle Hysteresis Increase by Trenches

The red and the black graphs on the figure 2.18 show the surface step profiles of the bare Molybdenum layer on the substrate and the surface of hydrophobic coated device with 300 μm finger width and 50 μm spacing, respectively. The measured thickness of the metal layer and the depth of trench were similar as 46.43 nm and 48.31 nm, respectively. This includes that the 0.9 μm-thick silicon oxide and 100 nm-thick hydrophobic coating layer coating did not fill trenches on metal layer. Thus, the surface roughness was increased by the trenches

Figure 2.19 (a) and (b) show the captures of the 10 μL droplets from CAH measurement instrument. The arrows mean the direction of droplet after tilting plate. Table 2.1 shows the measured average surface profiles, the standard deviation of height and root mean square (RMS) roughness of the devices. The all the average height results are in similar range of that of metal layer. Those results support that the trenches are not covered by thin film coating, even in case of aspect ratio of 22:1 between depths of trenches and thickness of thin films. With these chips, CAH was measured to investigate whether the number of trenches under contact line increase CAH. Figure 2.20 shows the relationship of the measured

CAH and the tilted angle that droplet starts to flow to the direction of the arrow. The graph shows CAH and tilted angle tended to increase with the number of trenches under contact line. Authors attribute the large standard deviation compared to increments of CAH is because the depth of trenches is as sallow as 48.31nm.

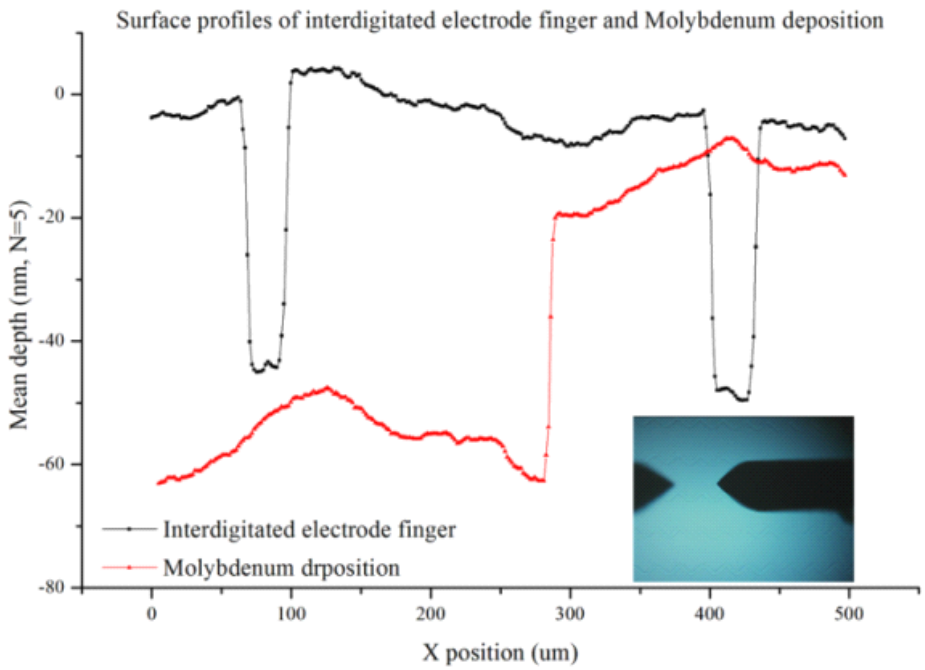

Figure 2.18 The surface profile of the interdigitated electrode pair including 300 um finger width and 50 um spacing (black) and the bare Molybdenum deposition (red). The inset is the captured image of the interdigitated electrode surface

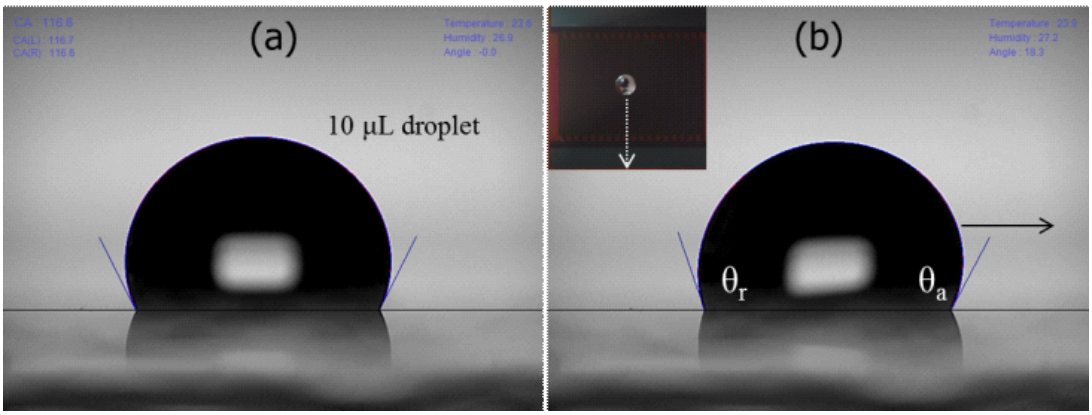

Figure 2.19 Images from contact angle hysteresis measurement device (a) 10 μL droplet was mounted by a pipette (b) distorted droplet shape by tilting chuck. θ_a, and θ_r mean advance and receding angle, respectively. The inset is the mounted interdigitated electrode device.

Electrode finger width (um)	300		500		800	
Electrode spacing (um)	30	50	30	50	30	50
Average height (nm)	44.49	48.31	44.14	43.24	47.97	40.78
Standard deviation (nm)	0.84	2.45	2.75	1.19	4.51	1.01
RMS roughness (nm)	2.04	5.35	9.62	8.05	8.15	13.64

Table 2.1. Depth of trenches between various electrode finger width and spacing.

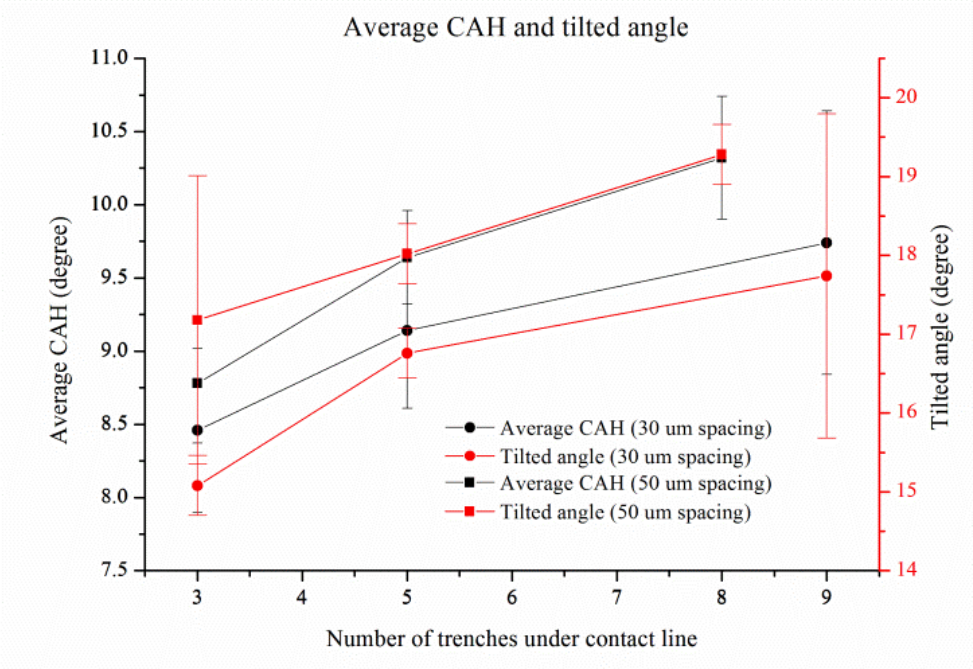

Figure 2.20 Trends of the average CAH and tilting angle with the change of the number of the trenches under contact line.

2.3.2 Surface Polishing Effect on Droplet Speed

To investigate the effect of removing trenches on droplet manipulation performance and reliability, maximum droplet speed and potential to generate electrolysis by dielectric breakdown were compared between the polished EWOD and the unpolished device. Figure 2.21 shows the surface profile graphs of the bare metal electrode, the polished EWOD device and the unpolished one with the black, the blue and the red lines, respectively. As well as the case of the interdigitated electrode devices, the trench on the unpolished EWOD device was not filled by deposition of insulating and hydrophobic coating layer. In case of the polished EWOD device, there was no trench between the electrodes, and additional slight roughness of 5.51 nm on the place that there was the trench. The trench depth of the unpolished EWOD case was 85.81 nm similar to 83.84 nm of the bare metal electrode. Figure 2.22 (a) ~(g) show the captures from video clips. In figure 2.22 (a), 5 μL droplets was manipulated with speed of 80 mm/s and 50 Hz of switching frequency on the polished EWOD device when 100 V was applied to activate the electrodes. In figure 2.16 (b), the droplet was manipulated with speed of 46 mm/s and 30 Hz switching frequency in the same experimental condition except for using the unpolished EWOD device. Table 2.2 shows summarized results of measuring maximum droplet speed. On 0.5×0.5 mm^2 electrode array of unpolished EWOD device, all the droplets of 1, 1.5 and 2.5 μL were pinned, but in case of the

polished EWOD device, they were manipulated with the speed of 33, 33 and 26 mm/s with 63, 63 and 50 Hz switching frequency, respectively. On 1×1 mm^2 electrode array of the unpolished EWOD device, 5 μL droplet was manipulated with speed of 21 mm/s, 20 Hz switching frequency and 7.5 μL droplet was pinned on the surface. In case of the polished EWOD device, 5 and 7.5 μL droplets were manipulated with speed of 35 mm/s, switching frequency of 33 Hz. On 1.5×1.5 mm^2 electrode array, 5, 7.5 and 10 μL droplets were tested. For the unpolished EWOD device, maximum manipulation speed of all the droplets was 46 mm/s with 30 Hz switching frequency. For the polished EWOD device, maximum speed for each volume of droplet were 80, 80 and 53 mm/s with 50, 50, 33 Hz switching frequency. Because the only difference in both devices was flattening the surface of the EWOD device, removing trenches critically affected improvement of droplet manipulation performance.

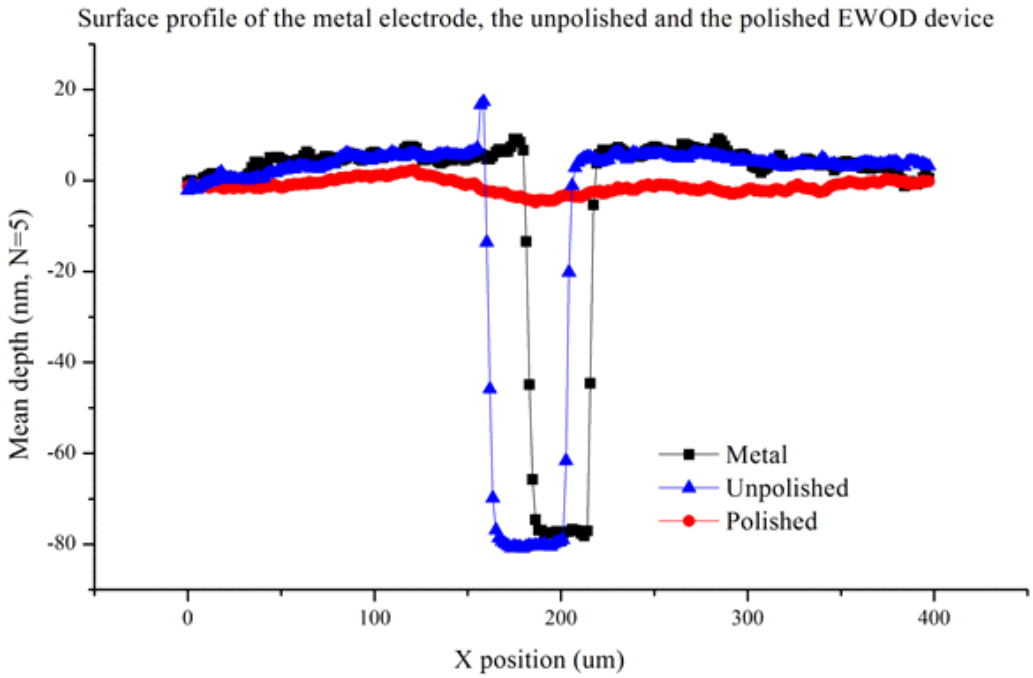

Figure 2.21 The surface profiles of bare metal electrode, the polished EWOD device and the unpolished one. The inset is capture from surface profiler.

Electrode Size (mm^2)	0.5 × 0.5 (25 μm gap)		1 × 1 (50 um gap)		1.5 × 1.5 (100 um gap)	
Fabrication method	Unpolished	Polished	Unpolished	Polished	Unpolished	Polished
Average height (nm)	85.81	2.09	87.04	3.70	88.44	5.48
Standard deviation (nm)	0.35	1.17	0.48	0.64	0.92	0.80
RMS Roughness factor (nm)	5.51	3.89	1.61	1.34	4.35	1.66

Table 2.2 Comparison of the surface profiles aquired from the Unpolished and the polished EWOD devices.

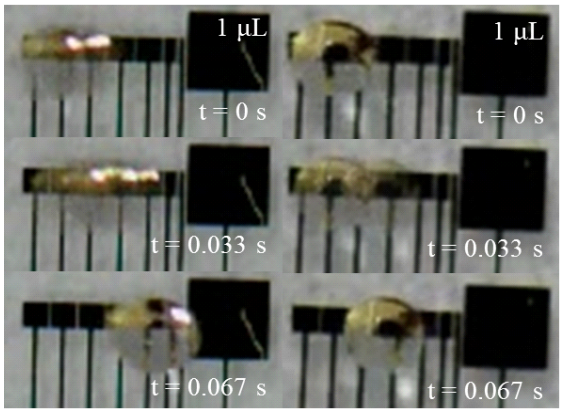
1 μL
t = 0 s
1 μL
t = 0 s
t = 0.033 s
t = 0.033 s
t = 0.067 s
t = 0.067 s

(a)

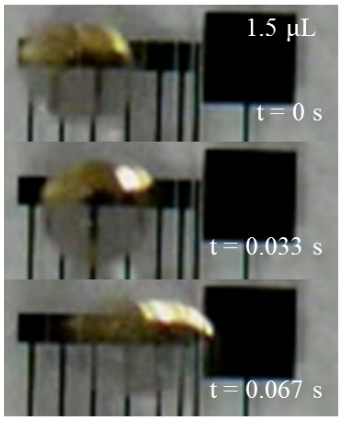
1.5 μL
t = 0 s
t = 0.033 s
t = 0.067 s

(b)

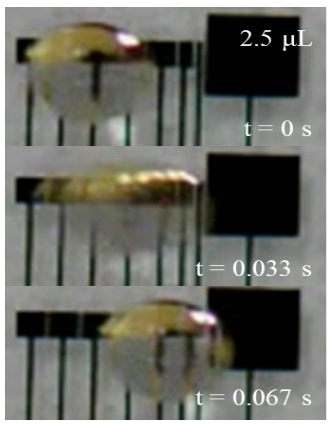
2.5 μL
t = 0 s
t = 0.033 s
t = 0.067 s

(c)

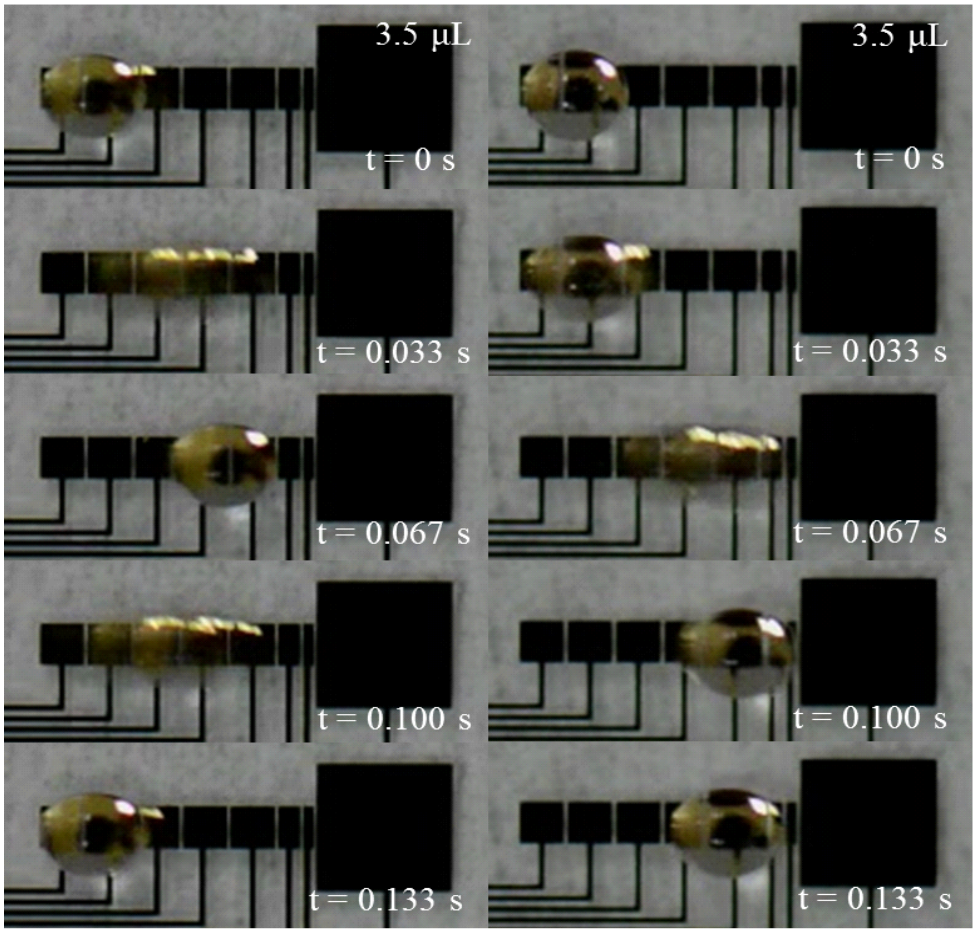
3.5 μL
t = 0 s
3.5 μL
t = 0 s
t = 0.033 s
t = 0.033 s
t = 0.067 s
t = 0.067 s
t = 0.100 s
t = 0.100 s
t = 0.133 s
t = 0.133 s

(d)

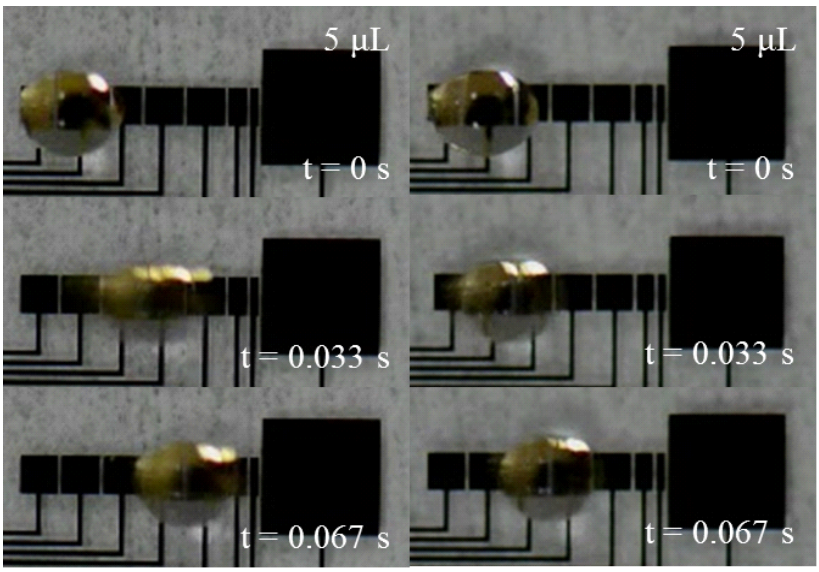
5 μL
t = 0 s
5 μL
t = 0 s
t = 0.033 s
t = 0.033 s
t = 0.067 s
t = 0.067 s

(e)

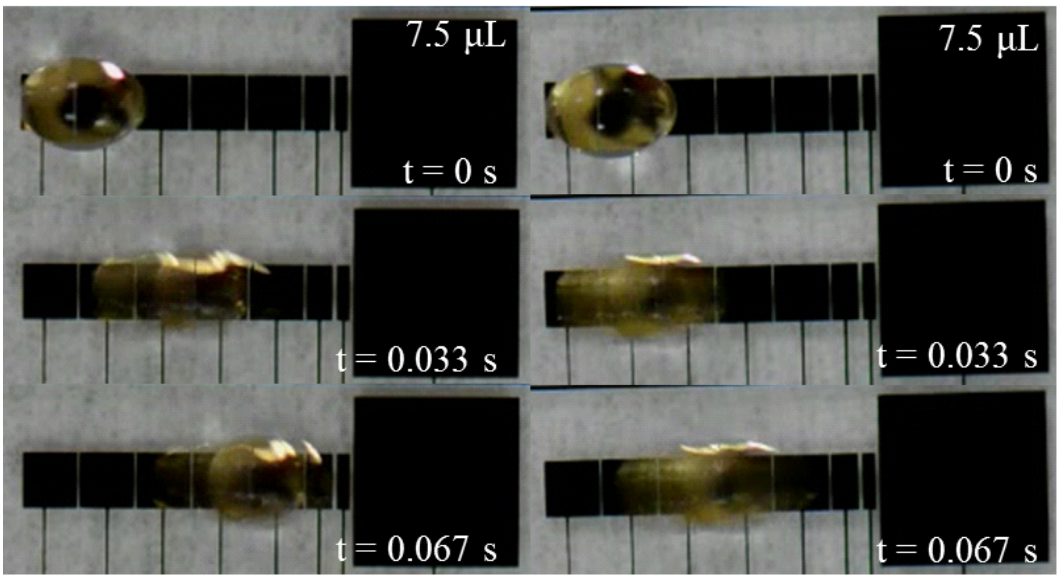
7.5 μL
t = 0 s
7.5 μL
t = 0 s
t = 0.033 s
t = 0.033 s
t = 0.067 s
t = 0.067 s

(f)

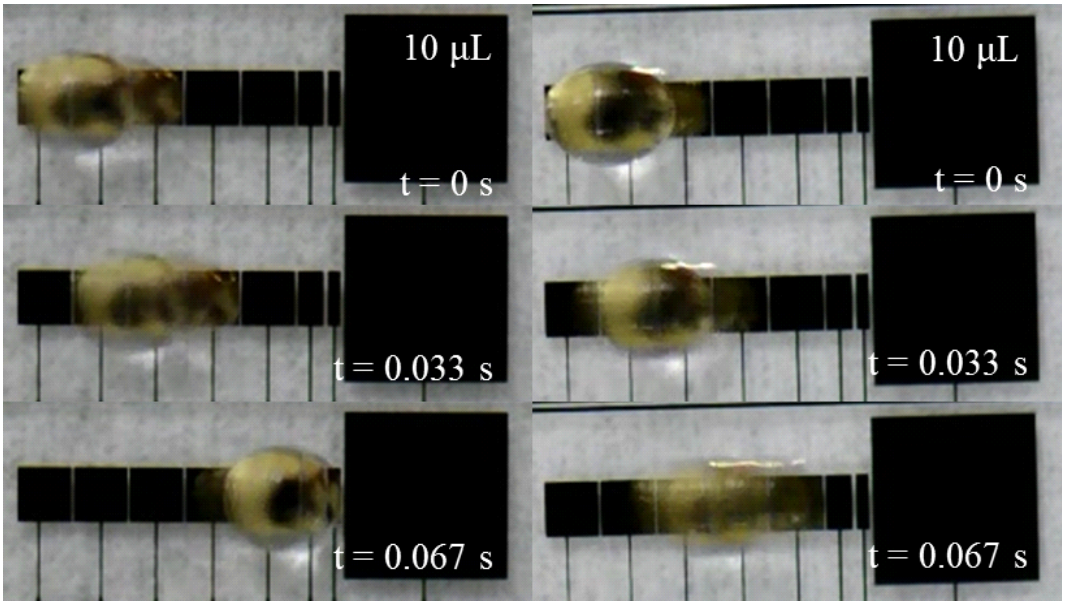

(g)

Figure 2.22 Captures from movies that includes droplet manipulation results presented in Table 2.3. (a), (b) and (c) were acquired from 0.5×0.5 mm^2 electrodes. (d) and (e) were from 1×1 mm^2 electrodes. (f) and (g) were attained from 1.5×1.5 mm^2 electrodes.

Electrode size (mm2)	Electrode gap (um)	Target volume (uL)	Unpolished (mm/s)	Polished (mm/s)	Enhancement (%)
0.5 x 0.5	25	1	21	33	57
		1.5	pinning	33	N/A
		2.5	pinning	26	N/A
1 x 1	50	3.5	35	70	100
		5	26	35	43
1.5 x 1.5	100	7.5	53	64	21
		10	53	64	21

Table 2.3 Droplet speed comparison between the unpolished and the polished EWOD device.

In table 2.3, the surface polishing effect on droplet speed enhancement was larger in experiments with small volume (<3.5 μL) than in those of the large (>3.5 μL). This can be explained by figure 2.23. Size of electrode in EWOD determines available volume range of droplet because contact line must be cover the electrode, which will be activated at the next sequence [31]. Main cause of interfering force against droplet movement is friction generated by droplet weight [32]. Trench length is dependent to electrode size, and this means the friction by trench is proportional to the electrode size. In the large droplet in figure 2.23 (a), the ratio of friction by trench and weight is F_t/F_w. On the other hand, the ration of friction by trench and weight in small droplet case is $\frac{1}{2}F_t \div \frac{1}{8}F_w = 4F_t/F_w$. Thus, the friction ratio of trench to weight is 4 fold in small droplet case compared to the large one. This is because relative high enhancement rate of droplet speed in small droplet case. the friction by trench is relatively large in small droplet. Table 2.4 summarized these explanation.

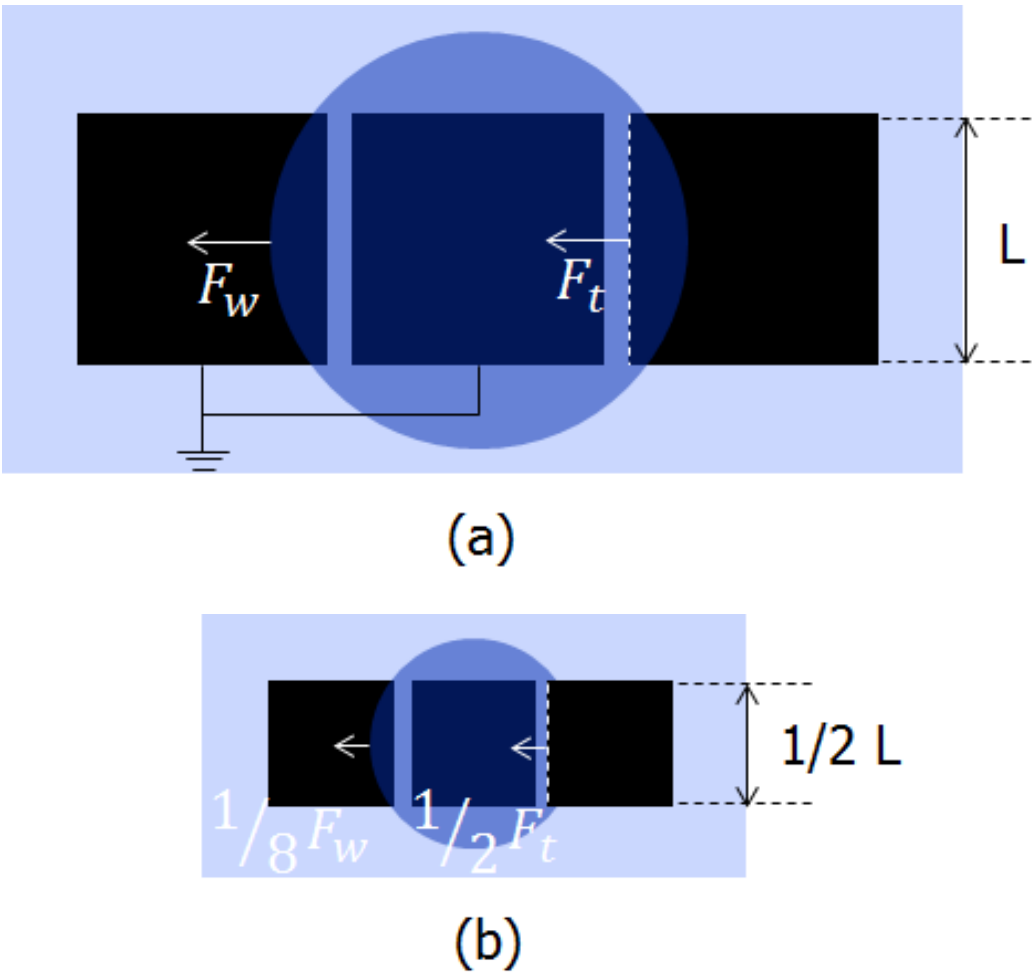

Figure 2.23 Comparison between the ratio of trench in total friction in large and small droplet.

Friction by	(a)	(b)
Weight	F_w	1/8 F_w
Trench	F_t	1/2 F_t
Trench/Weight	F_t/F_w	4 F_t/F_w

Table 2.4 Friction by droplet weight and trench. Droplet volume becomes smaller, the ratio of friction by trench in interfering force increases because the length of trench proportional to the electrode size.

2.3.3 Surface Polishing Effect on Breakdown Voltage

Defects on the surface of the EWOD device cause dielectric breakdown with low electric field intensity because thickness of thin films is slimmer than that of even surface. In this regards, dielectric breakdown occurs on the trench walls more frequently compared to the even areas of the electrodes because of imperfect step coverage. Figure 2.24 (a) and (b) show the pictures that potential of 140 V is applied to 1.5×1.5 mm^2 the electrodes in the polished EWOD and the unpolished one, respectively. On the polished EWOD device, droplet with a few tiny bubbles was stuck on the activated electrode, but severe electrolysis with generation of several bubbles was generated in the droplet on the unpolished EWOD device. This means that the polished EWOD device is more reliable than the unpolished one that has trenches vulnerable to be damaged by early dielectric breakdown.

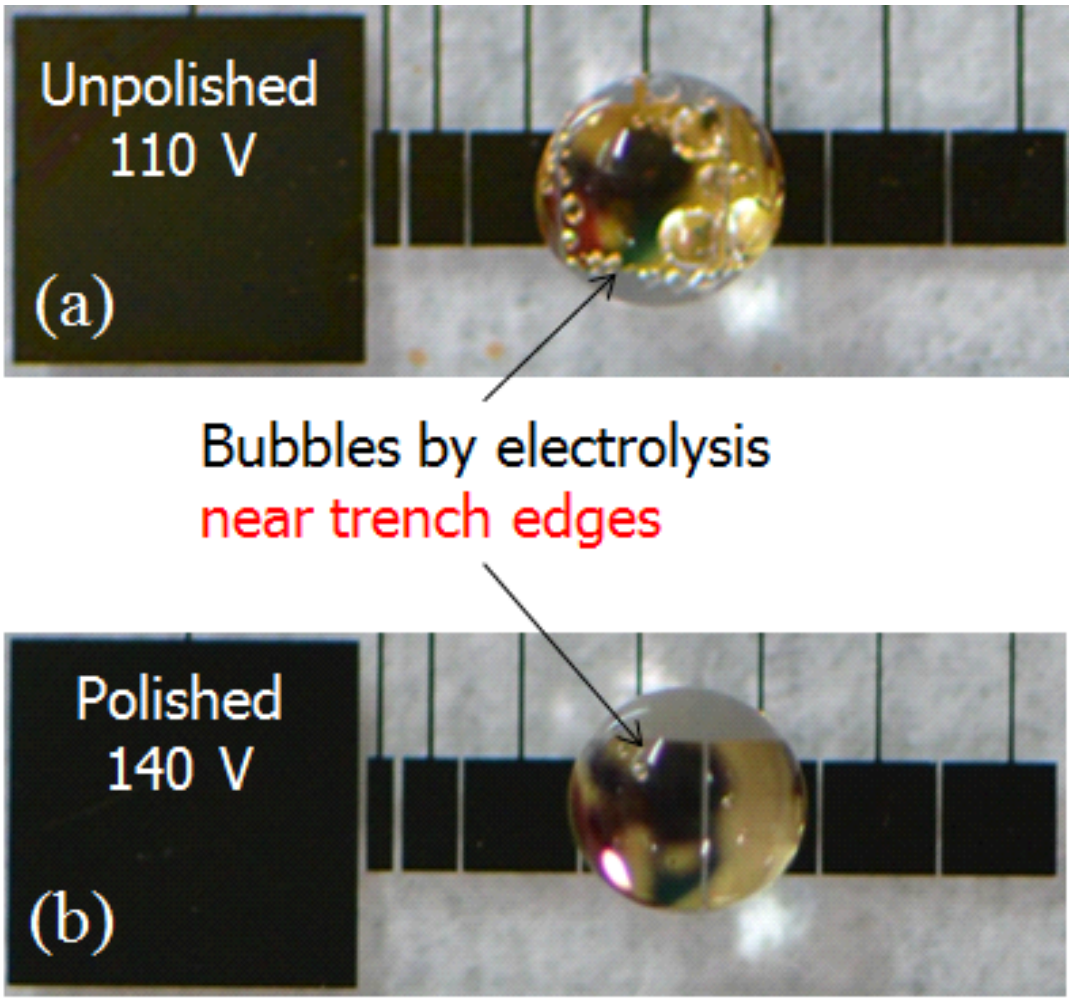

Figure 2.24 Captures from movies that includes droplet manipulation in (a) the polished and (b) the unpolished devices, respectively.

2.4 Conclusion

Trenches as thick as a metal electrode of EWOD device were verified experimentally. Adverse effects of trench was investigated by observing the relationship between the number of trenches under droplet contact line and CAH by tilting plate method. Thus, the unpolished and the polished EWOD device were fabricated and compared to each other for investigating whether removing trench enhance droplet speed and dielectric breakdown voltage. The result of these experiment showed that additional CMP technique in the EWOD fabrication could be a crucial procedure because of droplet performance enhancement and device reliability in the application which utilizes small volume (<1 μL) of droplets or requires extremely fast droplet manipulation.

Chapter 3

Surface Polishing Effect in Open OEW Device
Decrease of Droplet Heating

3.1 Introduction

3.1.1 Theory of Optoelectrowetting

From the first demonstration of light actuation of droplet in [15], many researchers started to find and develop application of optoelectrowetting (OEW) devices, because of the unique advantages. OEW device requires simple electrical wiring compared to EWOD devices. Only two feeding lines is utilized for applying AC signals to the interdigitated electrodes of the OEW device. In addition, on the OEW devices, droplets are able to be manipulated parallel and independently by illuminating light pattern. These two unique have

attracted the researchers who want to implement massive parallel bio-assay such as high throughput screening system [8]. Besides, OEW device inherently includes advantages of EWOD technology such as simple implementation, no requirement for pumps and valves and good reconfigurability.

As well as in EWOD operation, droplet are manipulated by applying electric field to droplet. However, difference is use of photoconductive layer under insulating layer in OEW device. Crystalline structure silicon dose not include significant photoconductive effect because electrons are bind with firmly organized silicon molecules like figure 3.1 [39]. In case of amorphous structure, electrons can easily be free from orbital of silicon molecules by transferring over energy of 1.1 eV (Energy difference between conduction and valence band) and they move to high potential site by repeating attachment and detachment to molecules around them. Because wave length ranging from near infrared to ultra violet ray include several eV of kinetic energy, charge-hole pair is generated in a-Si as shown in figure 3.1 (b). This let a-Si photoconductive character. Available resistance range of a-Si is shown in figure 3.2 [40]. Impedance model of OEW including a-Si layer is varied by illuminating light as shown in figure 3.3 (a) and (b) [15]. The insulating layer, a-Si and water can be modeled as C_{oxide} (capacitor), parallel $R_{aSi}C_{aSi}$ (Variable resistor and capacitor) and parallel R_wC_w, respectively. DC is not applicable to optoelectrowetting system because DC current cannot flow across the oxide layer. As a result

applied potential is totally dropped in the oxide layer in the circuit model in figure 3.3 (b). In dark, R_{aSi} ($10^{-8} S \cdot cm$) dominates C_{aSi}, resulting in almost of feeding potential is loaded to $R_{aSi.}$ With illumination, R_{aSi} increases order of 4 or 5, resulting in about $10^{-3} S \cdot cm$. Thus, C dominates and the situation is effectively same as the condition of reduced insulating layer thickness. as shown in 3.4.

Figure 3.5 show procedure that droplet is transported on the open OEW device. (a) First, droplet is mounted on the deivce. and it keeps hydrodynamic balance. (b) Second, AC potential is fed to the interdigitated electrode. Droplet does not change its shape because E-field is weak on this status because most of potential is loaded in a-Si layer (c) Third, if light is illuminated on the electrode, Resistance of a-Si is reduced by 5 order of magnitude and E-field on droplet strengthen. (d) By strengthened E-field, water molecules are polarized and charge is accumulated on the contact line by lightning rod effect. (e) By that strong, contact line front is pulled to the direction of electrode. (f) If contact angle of the droplet is changed, Pressure difference is generated and hydro dynamic force pulls the doplet to the direction of illuminated region.

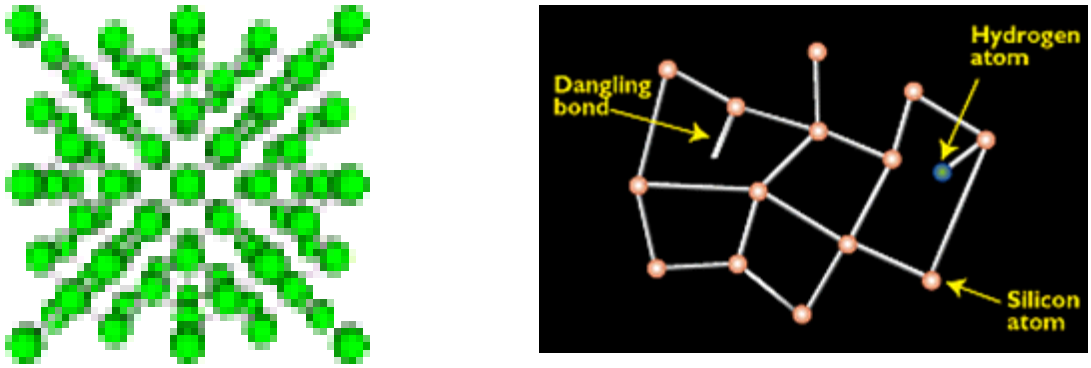

(a) (b)

Figure 3.1 Structure of (a) crystalline and (b) amorphous silicon [39].

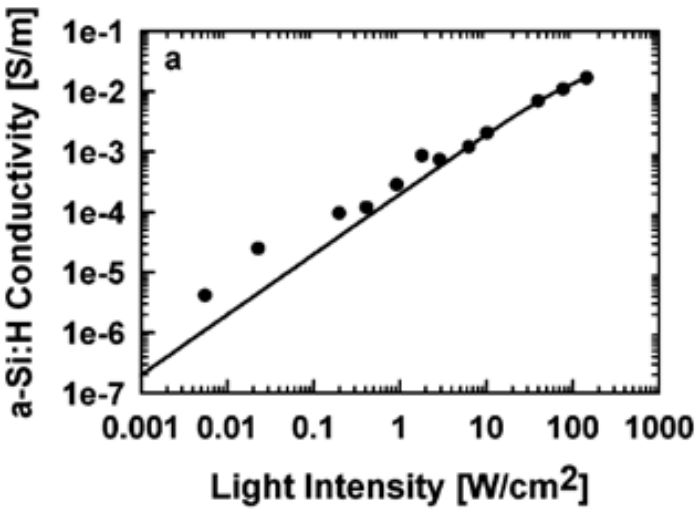

Figure 3.2 Available resistance range of a-Si [40].

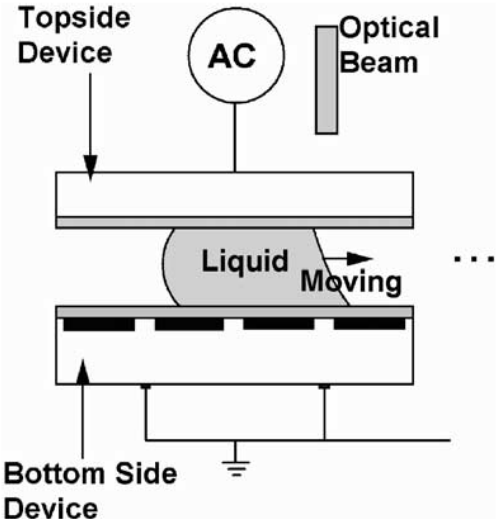

(a)

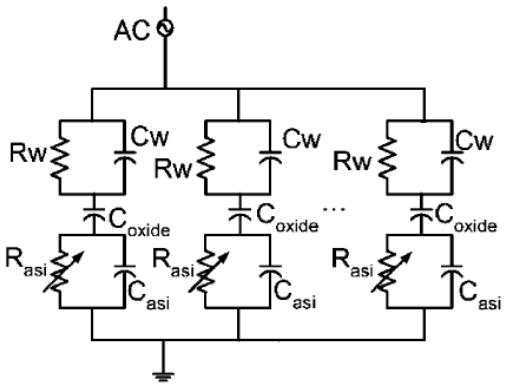

R_w, C_w: resistance and capacitance of water
C_{oxide}: capacitance of between liquid and electron
R_{asi}, C_{asi}: resistance and capacitance of amorphous Si

(b)

Figure 3.3 Schematic and impedance model of OEW device [15].

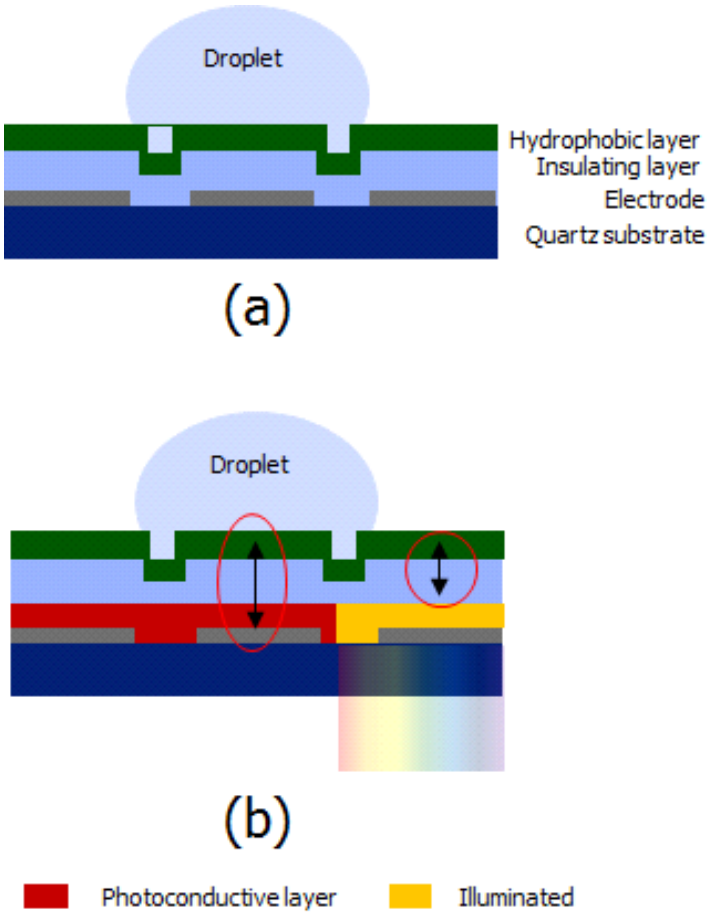

Figure 3.4 Difference between (a) EWOD and (b) OEW. In the EWOD structure, E-field is directly turned on/off by feeding electrode with software control. In the OEW structure, the photoconductive layer is changed from insulating-like to metal-like layer by illumination. In other words, photoconductive layer introduces the same effect that the insulating layer thickness is reduced.

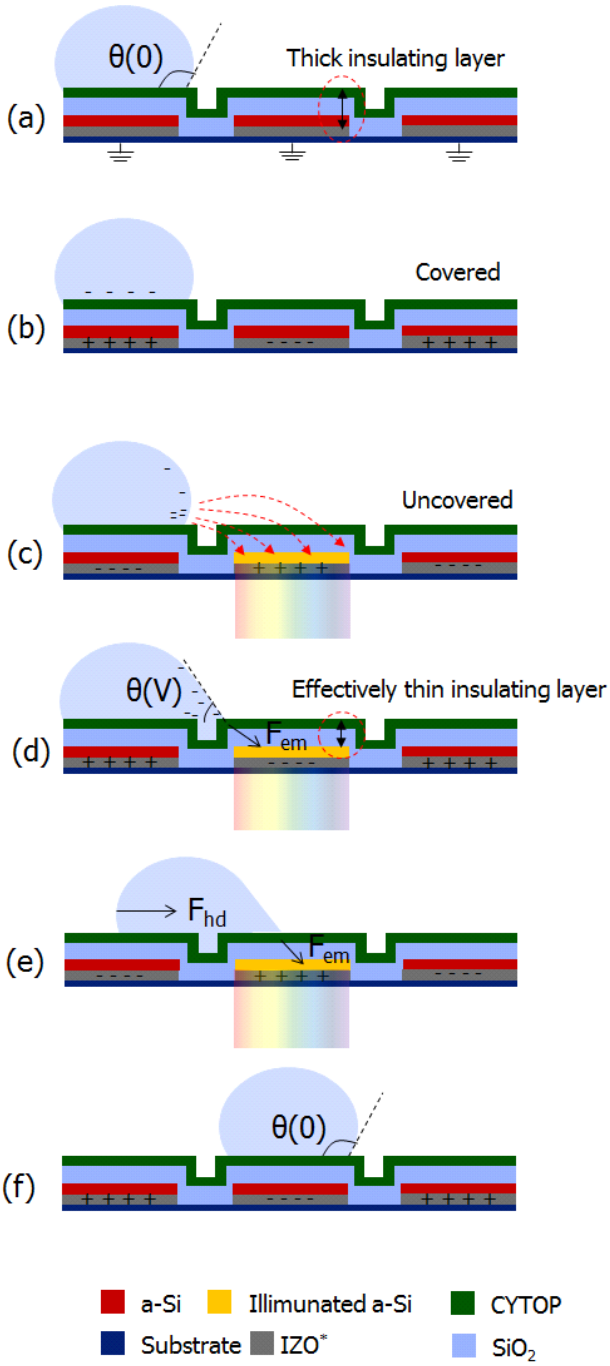

Figure 3.5 Procedure of droplet transportation.

3.1.2 Evaporation Issue on Small Droplet

Droplet evaporation is slow so that it is ignored in general [39]. In case of droplet over volume of 1uL, evaporation time takes 800 seconds as shown in 3.6. Also, if electrowetting device utilizes double plate or silicone oil as a medium, evaporation does not matter because evaporation rate is slow or silicone oil prevents it. However in case of open OEW targeting small droplet manipulation under 1 uL, evaporation would be serious because it changes concentration of sample in droplet. For example, 100 nL droplet takes 150 seconds to total evaporation following equation 3.1 in [1].

$$t = \frac{R^2}{D}\frac{\rho_{drop}}{C_v(1-H)} \qquad \text{(Equation 3.1)}$$

$t, R, D, \rho_{drop}, C_v$ and H are time for total evaporation, radius of droplet, diffusitivity of water vapor in air (26.1 mm^2/s), density of water, specific heat relative humidity. The droplet speed of the fastest open OEW device is 3.6 mm/s [41]. Thus it takes 30 seconds to transport 10 cm distance for droplet. This means about 20% of water droplet is evaporated in transport. In this regards, evaporation would one of important technical challenges for massive parallel bio-assay.

Thus, droplet heating is important issue because it accelerates droplet evaporation. Figure 3.7 shows relative evaporating rate of the upper droplet is faster than bottom because heat transfer

mechanismof the top and the bottom are convention to air and conduction to bottom. Thus, water molecule includes high energy on upper side. In this situation, volume of droplet is evaporated but, pinning if firm. This droplet pinned, resulting in contact angle decrease under 90°. The contact angle decrease in Young-Lippmann equation aggravates droplet transportation because it requires high electrowetting number to droplet movement.

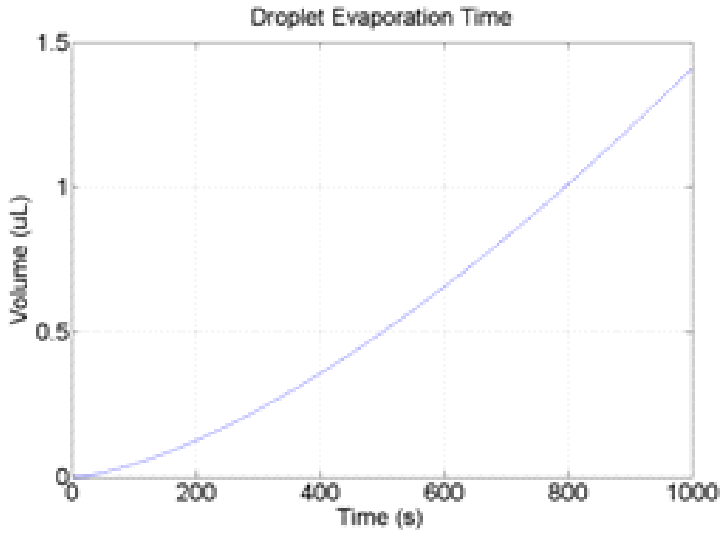

Figure 3.6 Evaporation time of small droplet [38].

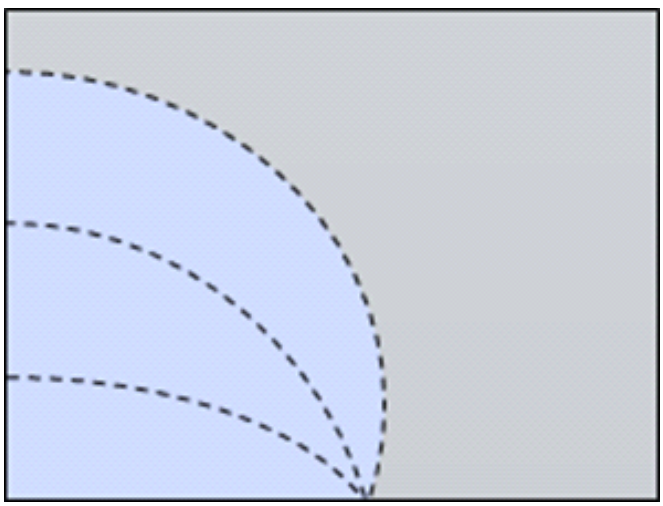

Figure 3.7 Contact angle decrease by droplet evaporation [42].

3.1.3 Goal of This Study

In this study, droplet heating is investigated in open OEW device. Because droplet is heated by resistive AC current flow in droplet and vibration [40]. This cause concentration and contact angle decrease problem as mentioned if droplet volume is under 1 μL. Thus, this chapter deals with droplet heating. Comparative study on a unpolished and a polished open OEW was fulfilled by measuring temperature of droplet with infrared thermal camera. The open OEW, which is not intensely used because of slow droplet speed and The reported 2-D open OEW is only one. Though heating is not illuminated as obstacle, it would be a challenge because researcher want to use small drop as possible. To prepare that, this study investigate relationship between droplet heating and evaporation by comparative study of the unpolished and the polished open OEW.

3.2 Experimental Section

3.2.1 Mask Design

To fabricate the unpolished and the polished open OEW device, the Cr mask was designed as shown in figure 3. 1 and 3. 2, respectively, because precise aligning is important factor for preventing device failure. Figure 3.1 shows the mask design of the unpolished open OEW. It includes the two interdigitated electrodes with 16 mm long and 300 um wide multi fingers. spacing between the fingers is 20 um. To improve capacitance between the interdigitated electrode and resolution of droplet transport, the edges of fingers are zigzagged shape. The interdigitated electrode of the polished open OEW device include similar one as the unpolished one. The dimension of the electrode fingers in the polished open OEW device was 240 um-wide with 20 um spacing. Both the open OEW devices were designed in 25×25 mm^2 square piece.

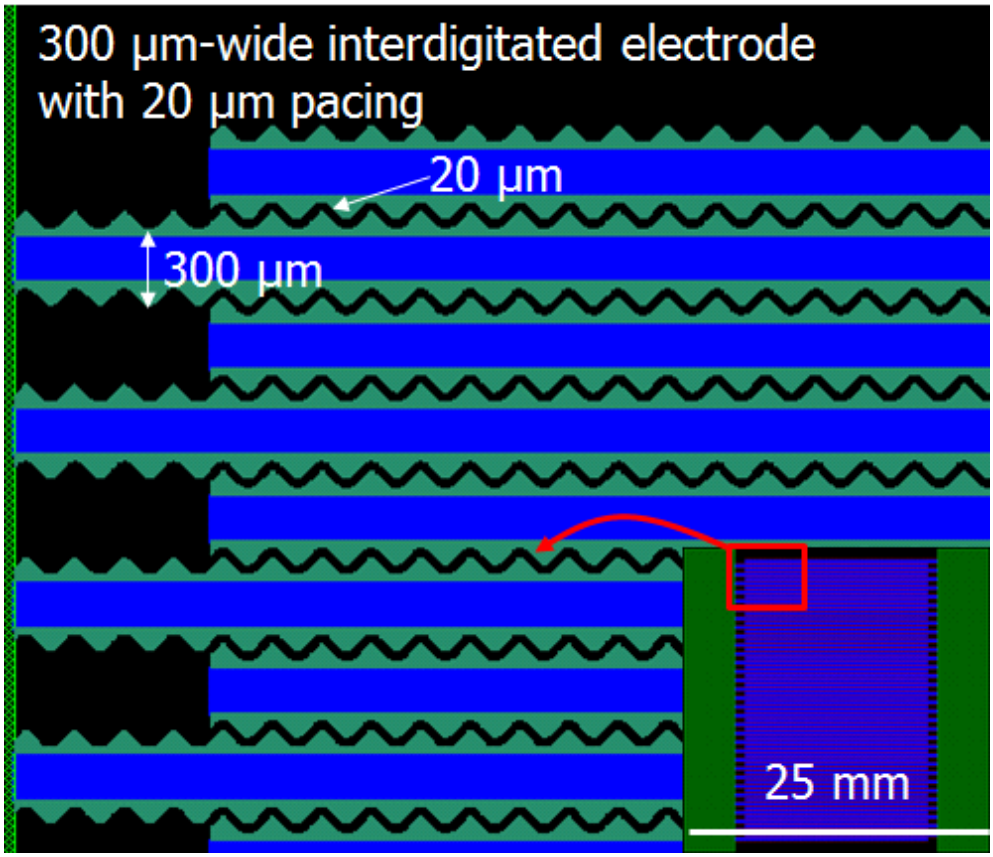

Figure 3.8 The mask design of the unpolished open OEW device.

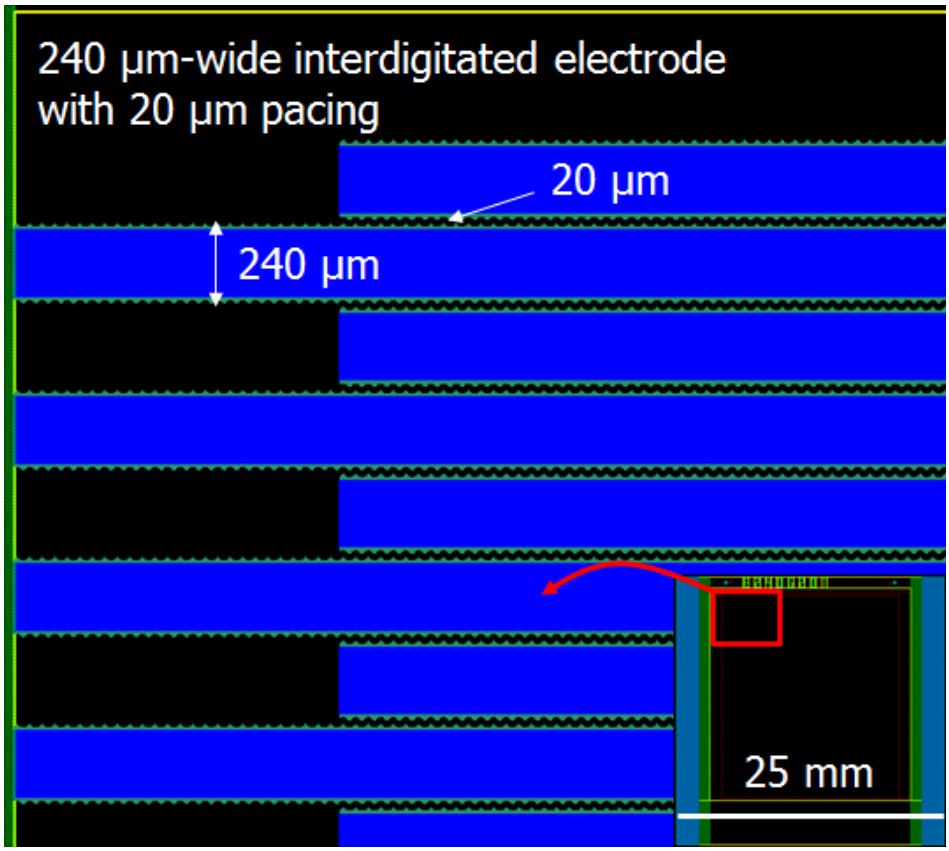

Figure 3.9 The mask design of the polished open OEW device.

3.2.2 Fabrication of a Unpolished and a Polished OEW Device

To comparative study on droplet heating by additional E-field by trench, a unpolished and a polished open OEW device were fabricated as figure 3.10 and 3.11, respectively. For fabricating the unpolished open OEW, On 6 inch glass rectangular substrate 50 nm-thick Molybdenum was deposited by sputter. To patterning electrode, positive photoresistor was spincoated follows by standard photolithography with the mask shown in figure 3.1. Then, Molybdenum was etched. Then, 400 nm-thick amorphous Silicon (a-Si) was deposited by plasma enhanced chemical vapor deposition (PECVD). As insulating layer, 500 nm-thick silicon dioxide (SiO_2) was deposited by PECVD. To reveal the feeding pad, SiO_2 and a-Si layer above that were etched by photolithography and reactive ion etching (RIE). Because the unpolished OEW device was 1×1 $inch^2$, 6 inch rectangular glass substrate was diced into 36 pieces of 1×1 $inch^2$ sample. (All above procedures were done in Advanced display research center of Kyounghee university). As the last step, diluted 100nm-thick CYTOP (1%) was spin-coated with 1000 rpm speed for 30 seconds as hydrophobic coating layer.

The polished open OEW was implemented as shown in figure 3.11. Indium Zinc oxide (IZO) was deposited on 6 inch quartz wafer, followed by 400 nm-thick a-Si. Photo-resistor was patterned by standard photolithography. Then, a-Si and IZO layer were patterned

by RIE (In ADRC of Kyounghee University). 1.5 um thick silicon dioxide layer was deposited by PECVD and upper 1 um of silicon dioxide layer was polished by CMP process (Interuniversity semiconductor research center of Seoul National University). The wafer was diced by 25×25 mm^2 and 100 nm-thick CYTOP was spin-coated. The inset image is photo of the open OEW device.

To verify whether the trenches are on the unpolished open OEW device, and no trench is on the polished open OEW device, the surface profile was measured. Figure 3.12 show the surface profile of both the devices. On the unpolished open OEW device, the 45 nm-deep trench was measured. On the polished open OEW device, there was no trench, but additional 5 nm roughness.

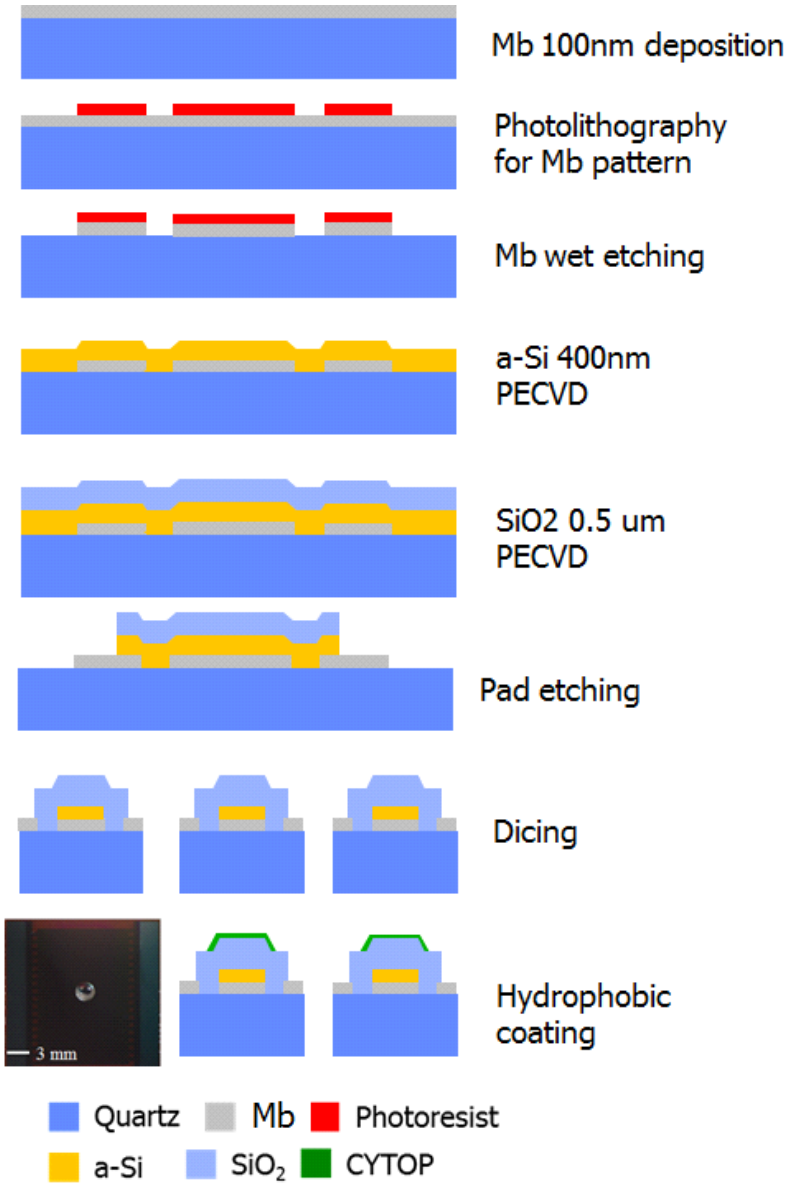

Figure 3.10 Fabrication procedure of the unpolished open OEW. The inset is the image of the fabricated device.

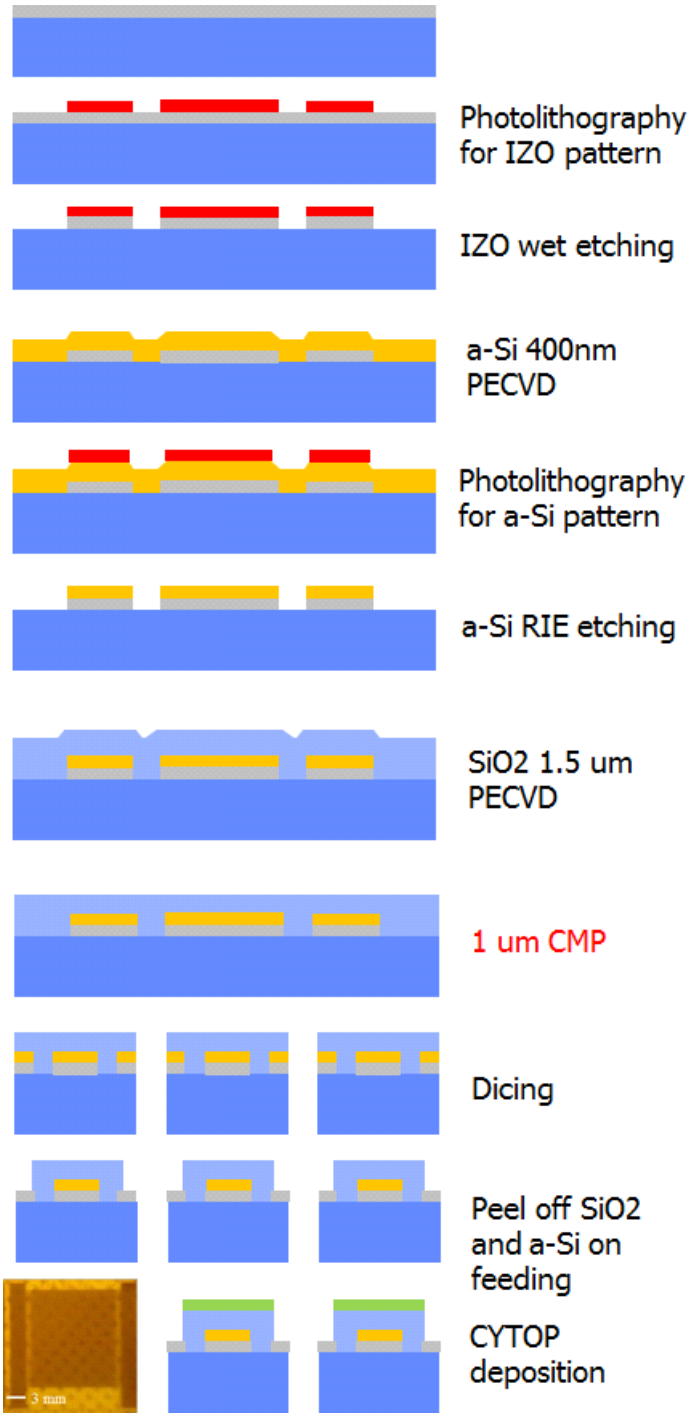

Figure 3.11 Fabrication procedure of the polished open OEW. The inset is the image of the fabricated device.

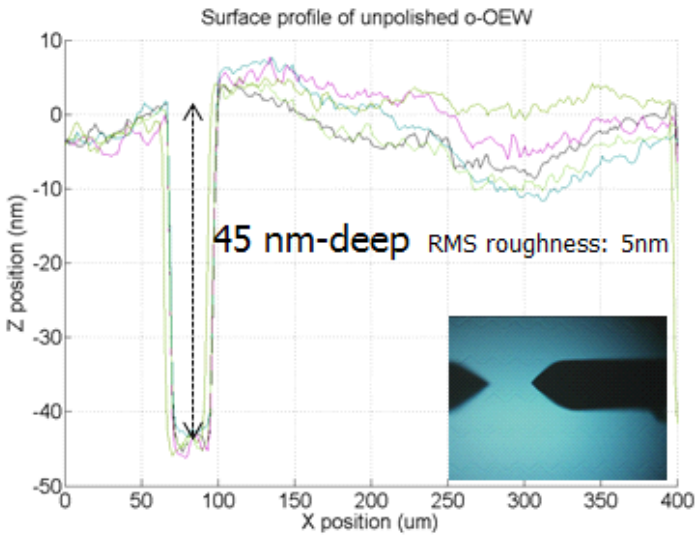

(a)

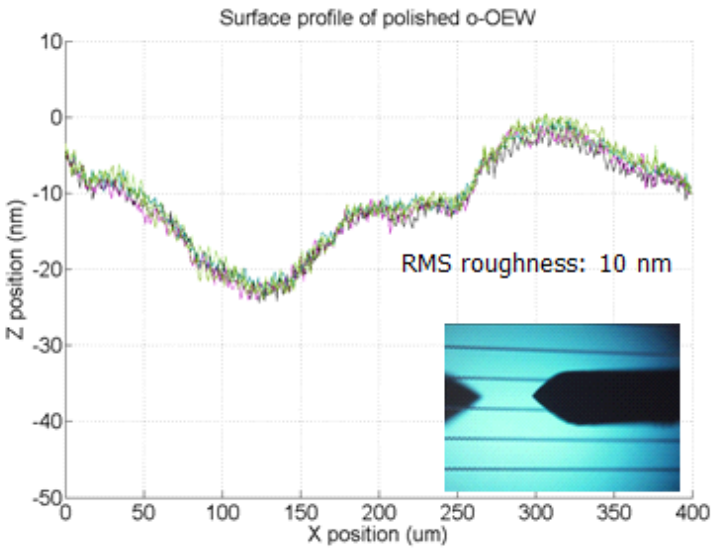

(b)

Figure 3.12 The surface profile measurement results of (a) the unpolished and (b) the polished open OEW. The depth of trench of the unpolished sample was 45 nm. There was no trench on the polished one, but 5 nm roughness.

3.2.3 Experimental Setup

Figure 3.13 shows the setup of droplet heating experiment. With a digital function generator and custom made high voltage amplifier, 180 V of 100 Hz sinusoidal signal was generated and parallel fed to the both the unpolished and the polished open OEW device. 10 uL droplet was mounted on both the devices and Thermal image was acquired by the IR camera (FLIR, Thermoscan e25, United States). After this experiment, hydrophobicity of the devices was tested to investigate whether temperature increase is caused by direct heating with dielectric breakdown.

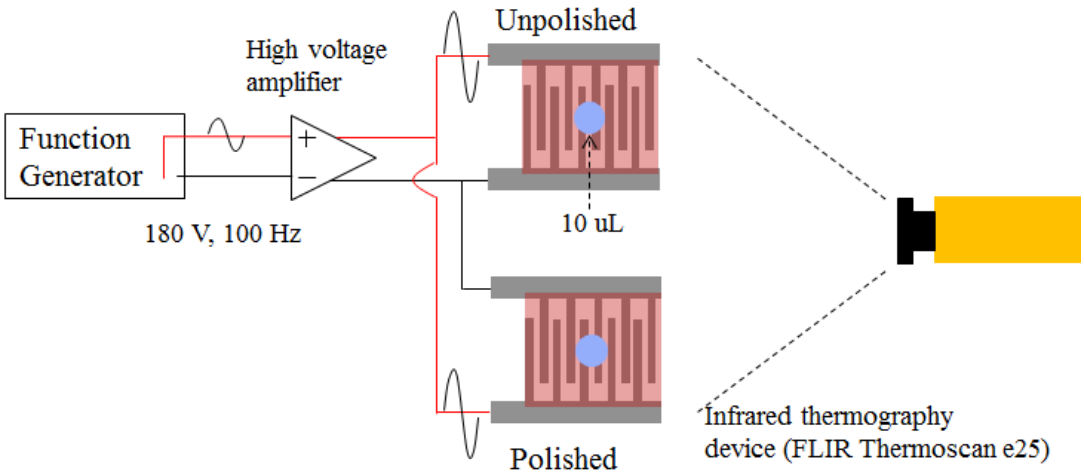

Figure 3.13 Fabrication procedure of the polished open OEW. The inset is the image of the fabricated device.

3.3 Results and Discussion

3.3.1 Surface Polishing Effect on Droplet Heating

The result of droplet heating test in figure 3.13. By applying 180 V of 100 Hz feeding voltage for 3 minutes, temperature of 10 uL droplet were heated from 25 °C to 35 °C on the unpolished open OEW, while no temperature increase on the polished sample. Temperature increase on the unpolished open OEW was because the strong E-field created by lightning rod effect on the trench edges. Also, thermal source was not resistive heating because there was not dielectric breakdown. It was verified that droplet contact angle was larger than 90° after temperature experiment.

Transferred heat was calculated using equation 3.2 with ignoring heat conduction between droplet and the device as well as heat convection between droplet and air.

$$Q = cm\triangle T \qquad \text{(Equation 3.2)}$$

where $Q(J)$, $c(4.181\frac{J}{g \cdot K})$ [40], $m(g)$ and $\triangle T(K)$ are transferred heat, specific heat of water, mass and temperature difference assuming that ambient temperature (25 °C). Transferred heat and power following by equation 3.2 were $41.8\mu J$ and $0.23\mu W$, respectively. This is minimum transferred energy and power. Thus,

more power would be transferred to the droplet on the unpolished open OEW device. The experiment was done in ambient environment with 5 nW of light intensity. Considering experimental condition that high energy laser (>25 mW) illuminates the a-Si layer which enable resistive conduction current flows, more heat would be transferred to droplet. In addition, This heat transfer would be a one of critical problems because it accelerates evaporation of small droplet [40].

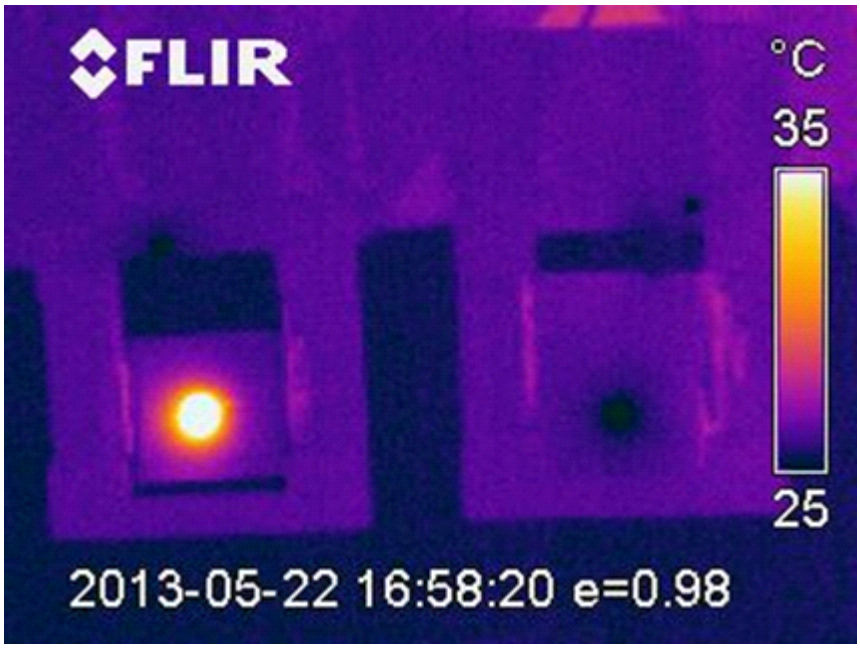

(a)

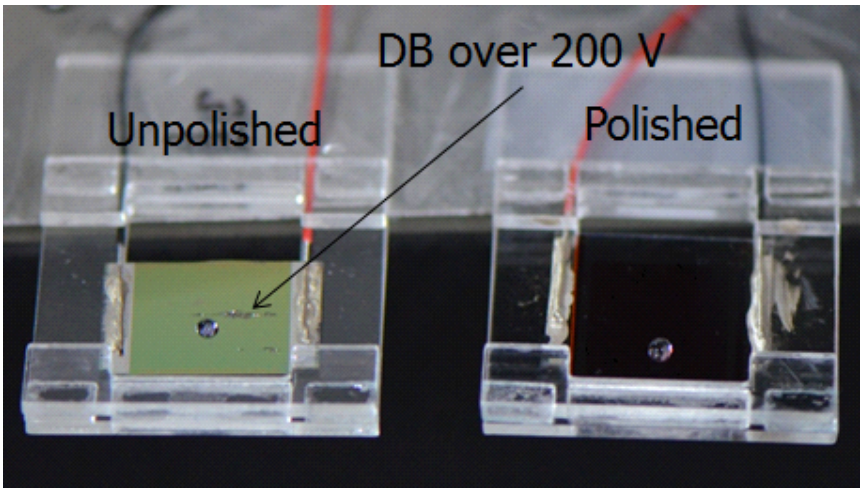

(b)

Figure 3.14 (a) Thermal image acquired from droplet heating experiment and (b) Image after heating experiment. The hydrophobic layer was not broken down based on the fact that the contact angle was larger than 90° on the unpolished open OEW device.

3.3.2 Evaporation Time of 1 μL Droplet by Potential Variation

Figure 3.15 shows the result of 1 μL (1.52 mm-wide) droplet evaporation time measurement. By Comparing figure 15 (a) and (b), reducing droplet heating by surface polishing is cleared. Figure 3.15 (a) was acquired when the experiment was started. Temperature of 1 μL droplet mounted on the unpolished and the polished OEW device were same each other. After 10 minutes with applying 192 V of 100 Hz sinusoidal signal, temperature of the droplet on the unpolished OEW was raised to ~28 °C and this was maintained until total evaporation. Also the droplet diameter of the polished in figure 3.15 (b) was 2.5 fold (1.12 mm-wide) compared to that of the unpolished one (0.64 mm). Because volume is proportional to cubic diameter of droplet, we can estimate difference of droplet evaporation rate is large enough to polish the surface eventought additional fabrication procedure.

Figure 3.16 shows the result of evaporation time measurement with supply voltage variation. Applied potential was 96 V to 192 V of 100 Hz. Total evaporation time was measured with thermal image. Because droplet heating is severe in high voltage range, evaporation time becomes shorter as potential grow large. Tendency of evaporation time was similar in the unpolished and the polished OEW. On the other hand, absolute time to evaporate droplet in the polished sample was always large and percentage increased time

becomes larger from 29 % to 92 %. This is because additional E-field intensity generated by lightning rod effect on the corner of trench.

The result of this experiment is important because it means that as droplet size becomes small, evaporation issue will be challenging obstacle for massive parallel bio-assay utilizing about 100 nL droplet. Also polishing trench was fundamental method to reduce evaporation because it is caused by resistive heating inner droplet, not conduction from substrate or air.

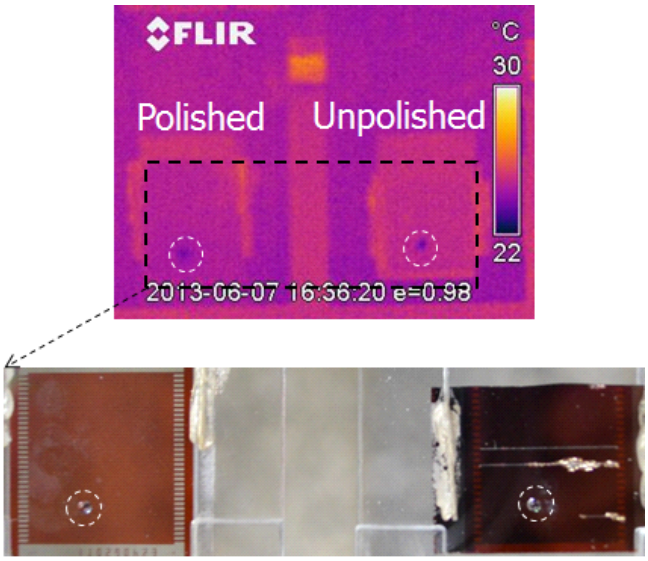

(a)

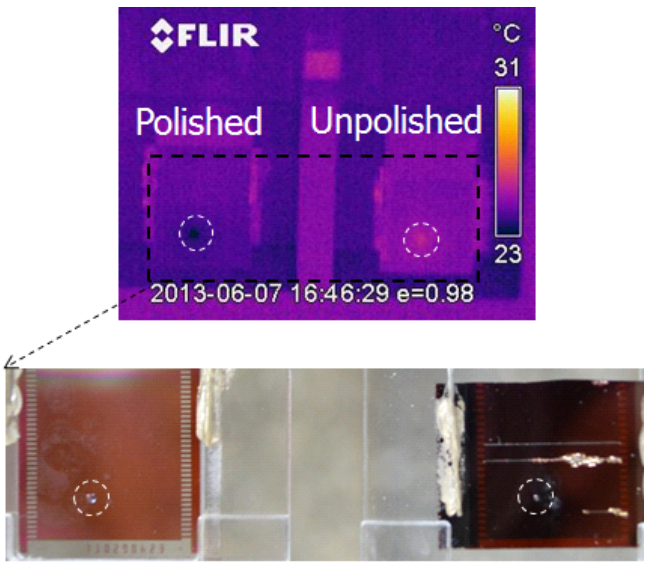

(b)

Figure 3.15 1 μL droplet evaporation test. (a) The Image acquired after start of experiment and (b) the picture attained after 10 minutes with 192 V potential with 100 Hz. Temperature difference was maintained by 6 °C until the end of the experiment.

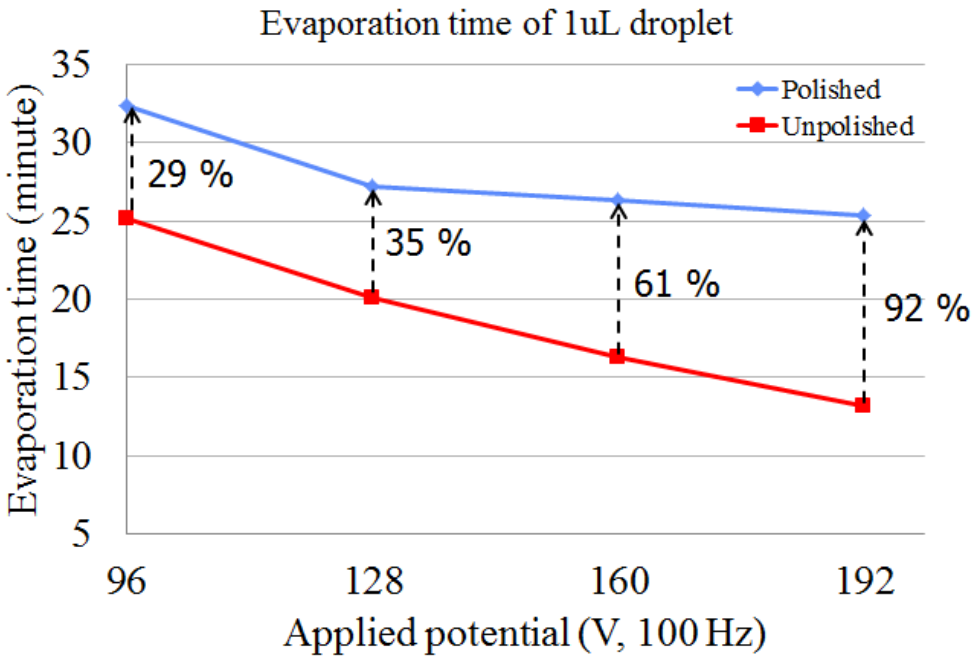

Figure 3.16 1 μL droplet evaporation test with activation potential variation. As expected, when relatively low potential was applied, droplet evaporation time was the longest as 25 min and 35 min in the unpolished and polished OEW, respectively. Because droplet heating rate on the unpolished OEW is larger than that in the polished one, evaporation time was increased from 29 % with 96 V activation to 92 % with 192 V.

3.4 Conslusion

Droplet heating is serious problematic when manipulating small droplet on open OEW device because intensive electric field is always applied to the device. Thus, droplet heating and evaporation experiments were done in this chapter to investigate whether surface polishing of open OEW device reduces droplet heating and evaporation. By applied 180 V of 100 Hz to 10 μL droplet on the unpolished and the polished OEW device, temperature difference was saturated at 10 °C. This result shows that additional E-field by lightning rod effect on trench edge accelerated droplet heating. Droplet evaporation experiment includes importance because it means that polishing trench becomes required as droplet is smaller. Especially in open optoelectrowetting device, high voltage feeding is required because of weak force to pull droplet. In this regard, importance of removing trench for reducing E-field under droplet becomes large when increasing parallelism of open OEW device.

Chapter 4

Summary and Conclusion

This dissertation is a study of surface polishing effect on electrowetting devices. Electrowetting technology is promising tool for implementing parallel bio-assay because it has many of advantages such as independent control using electrical addressing and reconfigurability by software control or optical image of activation.

Thus, we focused on improving droplet movement, device reliability and evaporation issue which can be potential technical barrier in case of small droplet use. By repeated experiments and trials, we found that intense electric field on trench edge is cause of droplet speed decrease, device damage by dielectric breakdown, and droplet heating. To resolve these problems, CMP was proposed as a method to remove trench to relieve electric field intensity.

To show that surface polishing relieves the problems, comparative studies were designed as comparing droplet speed and dielectric

breakdown of the unpolished and the polished EWOD device. With this study, we illuminated that the cause of droplet speed decrease and early dielectric breakdown is additional intensive E-field generated on the corner of the trench by lightning rod effect. As the first effect of surface polishing, droplet speed was improved up to 100 %. Especially, polishing was more effective. Ratio of trench in friction, interfering force, becomes larger in small droplet than in large droplet because friction by trench is reduced proportional to the electrode size, but friction by weight decreases proportional cubic of the electrode size.

As second effect of surface polishing, we verified increase of dielectric breakdown voltage. Because insulating and hydrophobic layer is thin film under 1 um-thick, dielectric breakdown is frequent cause of device damage. Even, deposition thickness in the trench edge is thinner than non edge region of the electrode because of low step coverage. This problem was also relieved by polishing that removing trenches. Dielectric breakdown voltage was enhanced from 100 V to 140 V (27 %). With E-field distribution result of simulation, we validated E-field intensity was reduced by polishing near trench.

As third effect of surface polishing, droplet heating was reduced. By evaporating 1 μL droplet with activation from 96 V to 200 V of 100 Hz, we verified that total evaporation time was elongated from 29 % up to 92 % with variation of supply voltage by removing trench. This is important in small droplet range because it takes several hundred seconds to evaporate 100 nano-liter level droplet. In addition,

droplet manipulation by electrowetting becomes impossible because of contact angle decrease by evaporation

Polishing is simple solution, but resolves fundamental problems related electrowetting device, especially in small droplet range. For cost effective analysis, droplet volume must be reduced, and this requires removing trenches to implement massive parallel bio-assay.

Bibliography

[1] R. B. Fair, "Digital microfluidics: is a true lab-on-a-chip possible?," Microfluidics and Nanofluidics, vol. 3, pp. 245-281, Jun 2007.

[2] A. Kumar, S. J. Williams, H. S. Chuang, N. G. Green, and S. T. Wereley, "Hybrid opto-electric manipulation in microfluidics-opportunities and challenges," Lab on a Chip, vol. 11, pp. 2135-2148, 2011.

[3] F. Mugele and J. C. Baret, "Electrowetting: From basics to applications," Journal of Physics-Condensed Matter, vol. 17, pp. R705-R774, Jul 20 2005.

[4] S. C. C. Shih, H. Yang, M. J. Jebrail, R. Fobel, N. McIntosh, O. Y. Al-Dirbashi, et al., "Dried Blood Spot Analysis by Digital Microfluidics Coupled to Nanoelectrospray Ionization Mass Spectrometry," Analytical Chemistry, vol. 84, pp. 3731-3738, Apr 17 2012.

[5] W. A. Schell, J. L. Benton, P. B. Smith, M. Poore, J. L. Rouse, D. J. Boles, et al., "Evaluation of a digital microfluidic real-time PCR platform to detect DNA of Candida albicans in blood," European Journal of Clinical Microbiology & Infectious Diseases, vol. 31, pp. 2237-2245, Sep 2012.

[6] B. Hadwen, G. R. Broder, D. Morganti, A. Jacobs, C. Brown, J. R. Hector, et al., "Programmable large area digital microfluidic array with integrated droplet sensing for bioassays," Lab on a Chip, vol. 12, pp. 3305-3313, 2012.

[7] S. K. Cho, Y. J. Zhao, and C. J. Kim, "Concentration and binary separation of micro particles for droplet-based digital microfluidics," Lab on a Chip, vol. 7, pp. 490-498, 2007.

[8] P. Y. Chiou, A. T. Ohta, and M. C. Wu, "Massively parallel

manipulation of single cells and microparticles using optical images," Nature, vol. 436, pp. 370-372, Jul 21 2005.

[9] H. Dahms, "Electrocapillary Measurements at the Interface Insulator Electrolytic Solution" J. Electrochem. Soc. 1969 116(11): 1532-1534.

[10] B. Berge, "Electrocapillarity and Wetting of Insulator Films by Water," Comptes Rendus De L Academie Des Sciences Serie Ii, vol. 317, pp. 157-163, Jul 22 1993.

[11] Washizu M., "Electrostatic actuation of liquid droplets for microreactor applications" IEEE Trans. Ind. Appl. Vol 34, pp. 732 - 737, 1998

[12] M. G. Pollack, R. B. Fair, and A. D. Shenderov, "Electrowetting-based actuation of liquid droplets for microfluidic applications," Applied Physics Letters, vol. 77, pp. 1725-1726, Sep 11 2000.

[13] P. Y. Chiou, H. Moon, H. Toshiyoshi, C. J. Kim, and M. C. Wu, "Light actuation of liquid by optoelectrowetting," Sensors and Actuators a-Physical, vol. 104, pp. 222-228, May 15 2003.

[14] P. Y. Chiou, S. Y. Park, and M. C. Wu, "Continuous optoelectrowetting for picoliter droplet manipulation," Applied Physics Letters, vol. 93, Dec 1 2008.

[15] S. Y. Park, M. A. Teitell, and E. P. Y. Chiou, "Single-sided continuous optoelectrowetting (SCOEW) for droplet manipulation with light patterns," Lab on a Chip, vol. 10, pp. 1655-1661, 2010.

[16] H. J. Ding, S. Sadeghi, G. J. Shah, S. P. Chen, P. Y. Keng, C. J. Kim, et al., "Accurate dispensing of volatile reagents on demand for chemical reactions in EWOD chips," Lab on a Chip, vol. 12, pp. 3331-3340, 2012.

[17] H. S. Chuang, A. Kumar, and S. T. Wereley, "Open optoelectrowetting droplet actuation," Applied Physics Letters, vol. 93, Aug 11 2008.

[18] S. Choi, Y. Kwon, Y. S. Choi, E. S. Kim, J. Bae, and J. Lee, "Improvement in the Breakdown Properties of Electrowetting Using

Polyelectrolyte Ionic Solution," Langmuir, vol. 29, pp. 501-509, Jan 2013.

[19] Asahi Glass, Technical information of CYTOP Retrieved May 28, 2013, from http://www.agcce.com/CYTOP/TechInfo.asp

[19] DuPont, Product information of Teflon AF Retrieved May 28, 2013, from http://www2.dupont.com/Teflon_Industrial/en_US/assets/downloads/h44587.pdf

[20] E. J. Terrell and C. F. Higgs, "Hydrodynamics of slurry flow in chemical mechanical polishing - A review," Journal of the Electrochemical Society, vol. 153, pp. K15-K22, 2006.

[21] S. K. Fan, H. P. Yang, and W. Y. Hsu, "Droplet-on-a-wristband: Chip-to-chip digital microfluidic interfaces between replaceable and flexible electrowetting modules," Lab on a Chip, vol. 11, pp. 343-347, 2011.

[22] B. Hadwen, G. R. Broder, D. Morganti, A. Jacobs, C. Brown, J. R. Hector, et al., "Programmable large area digital microfluidic array with integrated droplet sensing for bioassays," Lab on a Chip, vol. 12, pp. 3305-3313, 2012.

[23] M. Jonsson-Niedziolka, F. Lapierre, Y. Coffinier, S. J. Parry, F. Zoueshtiagh, T. Foat, et al., "EWOD driven cleaning of bioparticles on hydrophobic and superhydrophobic surfaces," Lab on a Chip, vol. 11, pp. 490-496, 2011.

[24] D. G. Lee, J. Park, J. Bae, and H. Y. Kim, "Dynamics of a microliquid prism actuated by electrowetting," Lab on a Chip, vol. 13, pp. 274-279, 2013.

[25] H. W. Lu, F. Bottausci, J. D. Fowler, A. L. Bertozzi, C. Meinhart, and C. J. Kim, "A study of EWOD-driven droplets by PIV investigation," Lab on a Chip, vol. 8, pp. 456-461, 2008.

[26] V. Schaller, A. Sanz-Velasco, A. Kalabukhov, J. F. Schneiderman, F.

Oisjoen, A. Jesorka, et al., "Towards an electrowetting-based digital microfluidic platform for magnetic immunoassays," Lab on a Chip, vol. 9, pp. 3433-3436, 2009.

[27] K. H. Kang, "How electrostatic fields change contact angle in electrowetting," Langmuir, vol. 18, pp. 10318-10322, Dec 24 2002.

[28] J. Zeng and T. Korsmeyer, "Principles of droplet electrohydro dynamics for lab-on-a-chip," Lab on a Chip, vol. 4, pp. 265-277, 2004.

[29] R. Gupta, D. M. Sheth, T. K. Boone, A. B. Sevilla, and J. Frechette, "Impact of Pinning of the Triple Contact Line on Electrowetting Performance," Langmuir, vol. 27, pp. 14923-14929, Dec 20 2011.

[30] J. K. Park, J. Ryu, B. C. Koo, S. Lee, and K. H. Kang, "How the change of contact angle occurs for an evaporating droplet: effect of impurity and attached water films," Soft Matter, vol. 8, pp. 11889-11896, 2012.

[31] J. H. Chang and J. J. Pak, "Effect of Contact Angle Hysteresis on Electrowetting Threshold for Droplet Transport," Journal of Adhesion Science and Technology, vol. 26, pp. 2105-2111, 2012.

[32] J. Berthier, P. Dubois, P. Clementz, P. Claustre, C. Peponnet, and Y. Fouillet, "Actuation potentials and capillary forces in electrowetting based microsysterns," Sensors and Actuators a-Physical, vol. 134, pp. 471-479, Mar 15 2007.

[33] F. Li and F. Mugele, "How to make sticky surfaces slippery: Contact angle hysteresis in electrowetting with alternating voltage," Applied Physics Letters, vol. 92, Jun 16 2008.

[34] H. B. Li and H. P. Fang, "Hysteresis and Saturation of Contact Angle in Electrowetting on a Dielectric Simulated by the Lattice Boltzmann Method," Journal of Adhesion Science and Technology, vol. 26, pp. 1873-1881, 2012.

[35] J. Gong and C. J. Kim, "Direct referencing two dimensional array digital microfluidics using multilayer printed circuit board," Journal of Microelectromechanical Systems, vol. 17, pp. 257-264, Apr 2008.

[36] J. Gong and C. J. Kim, "All-electronic droplet generation on-chip with real-time feedback control for EWOD digital microfluidics," Lab on a Chip, vol. 8, pp. 898-906, 2008.

[37] S. Choi, Y. Kwon, Y. S. Choi, E. S. Kim, J. Bae, and J. Lee, "Improvement in the Breakdown Properties of Electrowetting Using Polyelectrolyte Ionic Solution," Langmuir, vol. 29, pp. 501-509, Jan 2013.

[38] C. G. Cooney, C. Y. Chen, M. R. Emerling, A. Nadim, and J. D. Sterling, "Electrowetting droplet microfluidics on a single planar surface," Microfluidics and Nanofluidics, vol. 2, pp. 435-446, Sep 2006.

[39] Azonm.com, Photovoltaic Materials - Amorphous Silicon Retrieved May 28, 2013, from http://www.azom.com/article.aspx?ArticleID=1168.

[40] H. Hu and R. G. Larson, "Evaporation of a sessile droplet on a substrate," Journal of Physical Chemistry B, vol. 106, pp. 1334-1344, Feb 14 2002.

[41] H. S. Chuang, A. Kumar, and S. T. Wereley, "Open optoelectrowetting droplet actuation," *Applied Physics Letters,* vol. 93, Aug 11 2008.

[42] M. Abdelgawad, P. Park, and A. R. Wheeler, "Optimization of device geometry in single-plate digital microfluidics," *Journal of Applied Physics,* vol. 105, May 1 2009.

[43] J. H. Chang and J. J. Pak, "Effect of Contact Angle Hysteresis on Electrowetting Threshold for Droplet Transport," Journal of AdhesionScience and Technology, vol. 26, pp. 2105-2111, 2012.

국문 초록

모든 일렉트로웨팅 (Electrowetting) 장치에서 시료의 단위인 드랍릿 (Droplet) 은 전극과 소수성 박막 표면 사이에 인가된 전기장에 의해 조작되므로 장치의 표면 상태는 드랍릿 조작에 중요한 영향을 미친다. 일렉트로웨팅 장치의 불균일한 표면은 피뢰침 효과에 의한 강도 높은 전기장 발생의 원인으로 일렉트로웨팅 장치의 드랍릿의 조작 능력과 안정성을 저하시키고 드랍릿을 가열시켜 빠르게 증발시킨다. 일렉트로웨팅 장치의 제작 과정에서 두께 1 um 이하의 절연 박막과 소수성 박막을 도포하기 때문에 전극 패턴 간격은 공정 후에도 메워지지 않고 장치 표면에 전극 두께 깊이의 트렌치로 남는다. 이러한 트렌치의 모서리에서는 박막의 두께가 더욱 더 얇기 때문에 발생한 강력한 전기장이 드랍릿 속도 저하, 드랍릿 점착, 절연체 파괴, 드랍릿 가열의 원인이다.

본 논문에서는 트렌치가 발생시키는 문제들을 해결하기 위해 소수성 박막을 도포하기 전에 절연 박막을 평탄화 (Chemical mechanical polishing, CMP) 한 일렉트로웨팅 장치를 제안하였다. 트렌치를 제거하는 것이 드랍릿 조작능력과 안정성 향상에 미치는 영향을 알아보기 위해 평탄화 하지 않은 Electrowetting on Dielectric (EWOD) 장치와 평탄화한 EWOD 장치를 제작하였다. 각 EWOD 장치는 1 uL 에서 10 uL 까지 총 일곱 종류의 드랍릿 속도에 대한 평탄화의 효과를 검증하기 위하여 0.5 × 0.5 mm^2, 1 × 1 mm^2, 1.5 × 1.5 mm^2 크기의 전극 배열을 포함하였다. 드랍릿 속도 측정 실험결과, 평탄화 된 1 × 1 mm^2 의 전극 배열에서 3.5 uL 의 드랍릿을 70 mm/s 의 속력으로 조작하여 평탄화 되지 않은 장치에서 측정한 35 mm/s 의 속력에 비해 드랏립 속도가

100 % 향상되었다. 다른 크기의 EWOD 장치에서의 실험을 포함해 종합하면 평탄화를 통해 드랍릿의 속력을 최소 21 %에서 최대 100 % 까지 향상시켰다.

같은 EWOD 장치를 이용한 절연체 파괴 실험에서 절연체 파괴 전압이 평탄화 공정에 의하여 110 V에서 140 V 로 약 27 % 향상되었다. 절연체 파괴 전압 향상을 이론적으로 검증할 목적으로 시행한 시뮬레이션의 결과, 평탄화 되지 않은 장치의 트렌치 모서리에서 252 V/um, 평탄화 된 장치에서 146 V/um 으로 평탄화로 인해 전기장의 세기가 약 40 % 감소하였다. 따라서 트렌치를 제거하는 것이 EWOD 장치의 절연체 파괴 전압을 높일 수 있다는 것을 이론과 실험을 통해 확인하였다.

일렉트로웨팅 장치의 공급전원으로 교류전압을 쓸 경우 전기장이 드랍릿 내부를 가열시킬 수 있다. 드랏립 가열은 드랍릿이 충분히 클 경우 영향이 미미하지만 드랍릿의 부피가 1 μL 이하일 경우 증발이 시료의 농도변화와 접촉각 감소의 문제를 일으킨다. 표면 평탄화가 드랍릿의 가열을 방지하는 지 비교연구하기 위해 평탄화하지 않은 오픈 옵토일렉트로웨팅 (Open optoelectrowetting, o-OEW) 장치와 평탄화한 o-OEW 장치를 제작하였다. 두 장치를 100 Hz 의 96 V에서 192 V 전압원에 병렬로 연결한 후 1 uL의 드랍릿이 완전히 증발하기까지의 시간을 측정하였다. 이 실험의 결과, o-OEW 장치의 표면을 평탄화 함으로써 드랍릿의 증발시간이 29 %에서 92 % 까지 증가하는 것을 확인하였다.

키워드: 일렉트로웨팅 (EWOD), 옵토일렉트로웨팅 (OEW), 디지털 마이크로플루이딕스, 접촉각 이력, 병렬 생체 검정, 표면 평탄화

Student Number : 2009-30954

Acknowledgement

감사의 글

지난 11년 동안 서울대학교에서 있었던 모든 희로애락과 소중한 인연을 떠올리며 감사의 글을 적습니다. 우선 스승이신 김희찬 교수님께 존경을 표합니다. 연구실의 따듯한 울타리를 떠나려니, 교수님께서 학생들에게 베푸신 하해와 같은 은혜가 더 절실히 다가옵니다. 교수님 말씀 하나하나가 고민과 연단의 과정을 반복할 수 있도록 했고 그러한 훈련을 통해서 사회에 나가 정당한 방법으로 성공해 보리라는 마음을 품을 수 있었습니다. 사회를 위하여 앞으로도 젊은 저희에게 광야의 만나와 같은 가르침을 주실 것으로 믿습니다. 교수님 진심으로 감사드립니다. 김성완 교수님께서 연구함에 있어 학생들이 고민 끝에 얻은 결정들을 중요하게 여겨주셔서 저희들이 조금씩 스스로 성장하고 있다는 믿음을 갖게 해주셨습니다. 공식적인 자리에서는 프로답게, 사적인 자리에서는 친근하게 조언해 주셔서 일의 목적과 중요성에 대한 반추의 단초를 제공해 주셨습니다. 지도 학생이 아님에도 많은 가르침을 주신 김성완 교수님 감사드립니다. 천홍구 교수님께서는 저에게 연구 주제를 주시고 바이오멤스 분야에 빠르게 적응할 수 있도록 실험 하나하나 같이 해주시며 경험과 통찰을 전수해주셔서 감사드리고 있습니다. 교수님 덕분에 제가 활동할 수 있는 지계가 넓어질 수 있었습니다. 주세경 교수님, 늘 마음씨 좋은 형님처럼 친근하게 대해주시고 연구에 관한 한 적확한 조언을 주셔서 감사했습니다. 허동은 교수님, 학위 발표에 아낌없이 조언해 주셔서 감사합니다. 석사과정 은사님이신 서울대학교 전기공학부 권영우 교수님께 역시 깊은 감사의 말씀을 드립니다. 권영우 교수님 강한 교육 방침 덕에 학부 졸업하고 헤매기만 하던 제가 정신을 차리고 인간다워 질 수 있습니다.

제 삶에 없어서는 안 될 중요한 학형이 세 분 계십니다. 정진호 교수님께서는 석사과정 좋은 주제를 주셔서 많은 고민들을 했고 또한 직접적 가르침을 받을 수 있어서 돌이켜보면 너무나 감사했습니다만 제 표현이 부족했습니다. 다시

금 감사의 말씀을 드립니다. 제가 연구를 똑바로 하지 않으면 늘 '사자후'로 정신을 깨워주시고 본인의 지식과 경험을 아낌없이 체득시켜주셨던 최우열 형님과 까칠하시지만 실제로는 다정다감하게 그리고 깊이 있게 회로를 설명해 주시던 김영민 형님 감사합니다. 형님들처럼 박학다식하기 위해 귀한 말씀들을 연구노트에 적어가며 열심히 공부했습니다. 무엇을 원하든 이루어 지기를 바라오며 저의 손이 필요하실 때에 제가 꼭 도움이 되어드릴 수 있었으면 좋겠습니다.

박사과정에 들어와서 많은 조언과 도움을 주신 분들에게도 감사드립니다. 현중 형님, 현석 형님, 재민 형님께서 저의 우문에 항상 현답을 주셨으며 후배들의 고민을 같이 해주셔서 기로들에서 좋은 결정을 할 수 있었습니다. 상윤 형님께서는 좋은 아이디어로 자극을 주셨고 대인의 풍모를 배울 수 있어 좋았습니다. 광복형 때때로 진중하게 느슨하게 진심 어린 조언을 해주셔서 고맙습니다. 형 결혼식에 학위 준비하느라 못가서 너무너무 미안합니다. 같은 기수이고 고락을 함께 나눈 승우와 치열이에게 감사한 마음을 전합니다. 심란하고 괴로울 때 같이 고민해주고 옆에서 피식피식 힘내라며 같이 웃어줘서 여러 난관을 하나하나 시나브로 넘어 올 수 있었습니다. 윤서형, 졸업 준비할 때 제가 간과했던 부분을 잘 짚어주셔서 심사장에서 한꺼풀 덜 벗겨질 수 있었습니다. 늘 전적으로 저의 편이었던 일형형님, 재평이, 경우에게도 감사의 마음을 전합니다. 제가 실족해도 늘 곁에서 지켜봐 주셔서 정신적으로 재기할 수 있었습니다. 앞으로 같이 고생하며 목적을 향해 일보일보 전진했으면 좋겠습니다. 재간둥이 형선이와 기현이도 우울할 때 앞에서 재주를 부려주어 지루하지 않은 연구실 생활을 할 수 있었고 특히 형선이는 실험하는 데에 많은 도움을 주어서 고맙게 생각합니다. 연구실 생활을 함께 한 여류 연구원 지원, 인아, 지흠 같이 할 수 있어서 몹시 즐거웠습니다. 민양 형님, 선미 선배님 힘내시고 유종의 미를 거두시길 비랍니다. 선권형 회사에서 열심히 잘하고 계시다는 소식 들어서 저도 참 좋습니다. 종민형님 꼭 사업 번창하시고 만승이도 좋은 결과로 빠르게 냈으면 좋겠습니다. 대화는 많이 하지 못했지만 병욱이, 은제, 중우, 동헌, 치헌이 교수님 말씀 잘 듣고 훌륭한 연구 결과 내시기 바랍니다. 우리 MELab 원들 감사합니다.

힘든 석사과정을 함께한 인찬, 광록에게 고마움을 느낍니다. 모종의 의미로

는 선배같은 광록, 늘 공부하며 요즘 특히 약진하는 인찬이와 밤이나 낮이나 함께였던 우리의 시간이 있어서 늘 학교에 가고 싶었습니다. 또한 광하 덕분에 유쾌한 나날을 보냈습니다. 저를 친형처럼 챙겨주는 한주 덕에 문명인에 더 가까이 다가갈 수 있었고, 가족 아닌 누군가에게 소중한 사람임에 뿌듯함을 느낄 수 있었습니다. 멋'장'이 평우, 꿈에 관한 진지한 대화를 나눌 수 있어서 고맙습니다. '국민학교' 2학년부터 고등학교 졸업할 때까지 늘 함께 했고 또한 눈빛으로 서로의 마음을 볼 수 있는 벗 대석이와 지나치게 친해져 버린 대석이의 아내 지혜에게 감사와 축복을 전하며 친구처럼 연인처럼 사는 모습이 얼마나 좋고 아름다운 지 말해주고 싶었습니다. 알고 보면 머리 좋은 성호와 냉정한 남자 인구에게도 낯간지럽지만 없어서는 안될 소중한 친구라고 말해주고 싶습니다.

마지막으로 사랑하는 부모님, 형, 형수님, 누나, 매형, 나경이, 태경이 에게 형언할 수 없을 만큼 감사의 말씀을 전합니다. 어릴 때를 돌아보면 형과 누나는 늘 저에게 좋은 것을 양보했습니다. 형만 한 아우가 없다는 것을 철이 들어가면서 알게 되었습니다. 여느 집 남매들처럼 싸우지도 않고 막내의 땡깡과 고집을 넓은 마음으로 받아주어서 지금에 와서야 사무치는 고마움과 미안함을 느끼고 있습니다. 저희 형 누나와 결혼해서 잘 살고 계신 형수님과 매형도 항상 응원해 주셔서 감사하고, 여우같고 귀여운 나경이와 야무지고 예쁜 태경이 건강하게 잘 자라줬으면 좋겠습니다. 언제나 한량없는 사랑과 지지를 주시는 아버지, 어머니. 거칠고 모자른 제가 이만큼 해올 수 있었던 것은 오롯이 정직하고 성실한 충청도 양반 아버지와 늘 새벽에 나가 사랑하는 이들을 위하여 기도하는 어머니를 체험하며 자랐기 때문입니다. 금전으로 살 수 없고 실천으로만 보여줄 수 있는 교육을 받고 자라서 제 삶에 큰 영광이고 복입니다. 좋은 부모님을 둠에 있어 조물주께 감사할 따름입니다. 늘 말씀하신 대로 사회에 유익이 되는 사람이 되도록 하겠습니다. 우리가 같이 했던 고락이 이제 제법 추억으로 바뀌어가고 있는데 아버지, 어머니에 대한 저의 바람은 앞으로 그저 건강하고 즐겁게 사시는 것 입니다. 아버지, 어머니 고맙고, 미안하고, 깊이 사랑합니다.

- 2013 년 7월 24일 연건에서, 이충희 드림 -